Preprint

A global platform solution for Big Data in low-temperature thermochronology

Samuel C Boone[1,2], Fabian Kohlmann[3], Wayne Noble[3], Moritz Theile[3], Romain Beucher[4], Barry Kohn[1], Stijn Glorie[2], Martin Danišík[5], Renjie Zhou[6], Malcolm McMillan[1], Brent McInnes[5], Andrew Gleadow[1] and Angus Nixon[2]

[1]School of Geography, Earth and Atmospheric Sciences, The University of Melbourne, Melbourne, Victoria 3010, Australia.
[2]Department of Earth Sciences, University of Adelaide, Adelaide, SA 5005, Australia.
[3]Lithodat Pty Ltd, Melbourne, Victoria 3030, Australia.
[4]Australian National University, Research School of Earth Sciences, Canberra, Australia.
[5]John de Laeter Centre, Curtin University, Bentley, Western Australia 6102, Australia.
[6]University of Queensland, School of Earth and Environmental Sciences, Brisbane, Australia.

Corresponding author: Samuel C Boone, samuel.boone@unimelb.edu.au

---

This preprint has been submitted for publication in **Scientific Advances**. Please note, this preprint has not yet been peer-reviewed. The final published version of this paper may, therefore, have slightly different content. If accepted, the final version of this manuscript will be available via the 'Peer-reviewed Publication DOI' link on the right-hand side of the webpage. Please feel free to contact the authors; we welcome feedback. Thank you.

PREPRINT
A global platform solution for Big Data in low-temperature thermochronology

Samuel C Boone[1,2], Fabian Kohlmann[3], Wayne Noble[3], Moritz Theile[3], Romain Beucher[4], Barry Kohn[1], Stijn Glorie[2], Martin Danišík[5], Renjie Zhou[6], Malcolm McMillan[1], Brent McInnes[5], Andrew Gleadow[1] and Angus Nixon[2]

[1]School of Geography, Earth and Atmospheric Sciences, The University of Melbourne, Melbourne, Victoria 3010, Australia.

[2]Department of Earth Sciences, University of Adelaide, Adelaide, SA 5005, Australia.
[3]Lithodat Pty Ltd, Melbourne, Victoria 3030, Australia.
[4]Australian National University, Research School of Earth Sciences, Canberra, Australia.
[5]John de Laeter Centre, Curtin University, Bentley, Western Australia 6102, Australia.
[6]University of Queensland, School of Earth and Environmental Sciences, Brisbane, Australia.

Abstract
Low-temperature thermochronology is a powerful tool for constraining the thermal evolution of geological materials at temperatures (< ~300 °C) common in the upper crust in relation to geodynamics, continental crustal evolution, landscape evolution, and natural resource formation and preservation. However, complexities inherent to these analytical techniques can make interpreting the significance of results challenging, requiring them to be placed in their geological context through time.

We present a novel tool for the geospatial archival, analysis and dissemination of low-temperature thermochronology data (i.e., fission track and (U-Th)/He), built as an extension to the open-access *AusGeochem* platform (https://ausgeochem.auscope.org.au) and which is freely accessible to scientists from around the world. To demonstrate the power and utility of the platform, three regional low-temperature thermochronology datasets from Kenya, Australia and the Red Sea are presented. By visualising and interrogating these data in their regional three-dimensional geological, geochemical, and geographic contexts, insights into their tectonic implications are revealed which could otherwise be overlooked.

Introduction
Low-temperature thermochronology encompasses a group of temperature-sensitive radiometric dating techniques which provide unique insights into the thermal history of Earth's upper crust. These observations, in turn, allow scientists to constrain the timing and rate of a breadth of geological processes which can affect the thermal state of the crust over geological time, including the advection of mass and heat due to the growth of mountain belts, extensional basin formation, and long-term denudation (*1*–*4*). Consequently, low-temperature thermochronology is an important tool for studying surface weathering processes (*e.g.*, *5*), paleoclimate (*e.g.*, *6*–*8*), and climate change (*e.g.*, *9*, *10*), as well as for constraining the formation and preservation of various natural resources, such as hydrocarbons (*11*, *12*), hydrothermal and supergene ore deposits (*13*–*16*), and geothermal energy fields (*17*, *18*). In certain instances, such analyses can even record thermal events related to localised conductive heat transfer related to igneous activity (*19*), volcanic eruptions (*20*, *21*), groundwater advection (*22*, *23*), hydrothermal fluid flow (*24*), wildfires (*25*), or meteorite formation (*26*). These insights into the thermal history of the crust reflect the geodynamic, tectonic, magmatic and surficial processes which govern the evolution of our planet's asthenosphere, lithosphere, biosphere and atmosphere.

The most commonly used low-temperature thermochronometers are the fission-track and (U-Th)/He methodologies. Like all absolute radiometric dating techniques, these systems are based on the radioactive decay of certain unstable isotope(s) to their decay product(s) at a known rate over geological time. The fission-track system, for example, is based on the formation and accumulation of microscopic damage trails (called fission tracks) in mineral grain crystal lattices due to the spontaneous fission of ^{238}U atoms (*27*), and the subsequent repair of these tracks via thermal annealing (*28*). The (U-Th)/He system is based on the production of alpha particles (^{4}He) in mineral grains during the decay chains of ^{238}U, ^{235}U, and ^{232}Th, and the loss of ^{4}He by thermally activated volume diffusion (*29*). However, unlike some higher-temperature geochronology systems, such as the U-Pb or Lu-Hf systems, whose systems can be considered closed at temperatures near or above those at which the analysed geological material has crystallised or lithified (*30*), the retention of the decay products (i.e., fission tracks and ^{4}He) of low-temperature thermochronometers remain sensitive at low temperatures at which crustal and near-surface geological processes occur (from ~300 °C down to ambient temperatures depending on the mineral in question, e.g., apatite, zircon, titanite, monazite, *29*, *31*, *32*). The temperature sensitivities of the fission-track and (U-Th)/He methods are further complicated by their dependence on other variables, such as cooling rate, mineral chemistry, crystal size, and radiation damage accumulation (*33*–*36*). As a result, apparent ages (dates) produced by thermochronometers may not correspond to distinct geological events. Rather, these thermochronological data often require integration with additional measurements of kinetic parameters (*33*, *37*–*40*) and numerical modelling (*41*), often using thermal history modelling software (*42*, *43*), to unravel and quantify the thermal histories that they record.

Consequently, interpreting the geological significance of thermal histories recorded by complex low-temperature thermochronology data requires placing those results in their three-dimensional geochemical, geospatial, geological, and geographic context through time. These data must, therefore, be interrogated in the context of previously acquired analyses, other related geochemistry data, local geology, and modern topography. This work generally involves laborious data mining from publications and disparate repositories into private data models, bespoke to an individual analyst or research group. In the current low-temperature thermochronology data ecosystem, all of these laborious data management and synthesis tasks must then be repeated for each new study region and by each subsequent geoscientist wishing to work in that particular area. While the number of samples with low-temperature thermochronology analyses for any given region may be modest, perhaps on the order of a few thousand per continent, the variety and volume of detailed (meta-)data attributes associated with each of these results (e.g., typically > 3000 for a single apatite fission track age comprising 30 single grains and 100 confined track lengths – see Supplementary Information) and the increasing rate at which these analyses are being produced make these traditional data processing workflows ineffectual. Even in the rare instances that such low-temperature thermochronology data syntheses are published in scientific journals or data repositories, they often remain unintelligible to non-specialists due to the inherent complexities of these methodologies. Thus, new intuitive tools are needed to enable the wider geoscience community to interrogate and understand these powerful datasets.

Here, we present a novel tool for efficient geospatial examination and dissemination of global fission-track and (U-Th)/He Big Data. This robust relational low-temperature thermochronology database is an extension of the open *AusGeochem* geochemistry data platform, https://ausgeochem.auscope.org.au (*44*), which enables users to upload, disseminate, interrogate, and publicise geosample metadata and secondary ion mass spectrometry U-Pb data in a geospatial context. The structured archival of detailed low-temperature thermochronology analyses in relational schemas, including fine-grained data on the individual crystal-, spot-, and track-scale (Supplementary Materials), facilitates rapid derivation of inter-data relationships, permitting data compilation, analysis, and visualisation of thousands of analyses generated by laboratories across the globe in real-time. As such, this *AusGeochem* extension presents the low-temperature thermochronology community with an unprecedented instrument for FAIR (Findable, Accessible, Interoperable, Reusable, *45*, *46*) fission-track and (U-Th)/He data management and Big Data investigation.

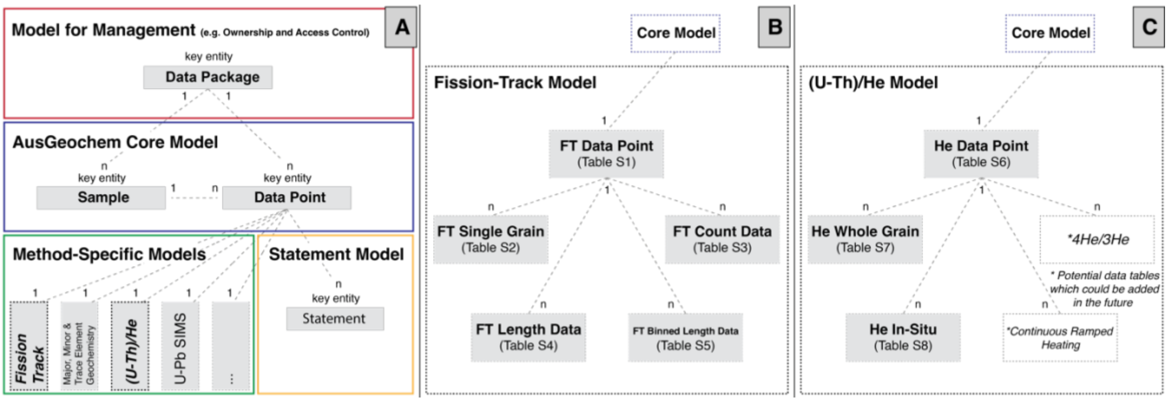

Fig. 1. Database architecture overview of AusGeochem (A), the fission-track data model (B) and the (U-Th)/He data model (C). Each object within the fission-track and (U-Th)/He model represents a data table, the details of which are presented in the Supplementary Information.

Results

The relational low-temperature thermochronology database architecture of *AusGeochem* (Fig. 1) enables users to geospatially interrogate data in ways not possible using existing data portals and repositories. While existing portal and repository data model architectures constrain the user's interaction with data to simply viewing and extracting(*47*), the structured and standardised way in which fission-track and (U-Th)/He analyses are stored in *AusGeochem* enables live cross-data analytics to be performed within the platform (*44*). The persistent data structure also allows for potential future developments for performing real-time computing, such as the recalculation of ages based on updated decay constants, bulk thermal history modelling of regional data sets, and viewing data in their palinspastic context.

AusGeochem provides users with two interfaces to interact with data (Fig. 2): My Data, where data can be managed, and Map View, where samples and analyses can be explored geospatially. Video tutorials on how to use *AusGeochem* can be found in the User Guide section of the platform's Help tab, or here: https://www.auscope.org.au/ausgeochem-help

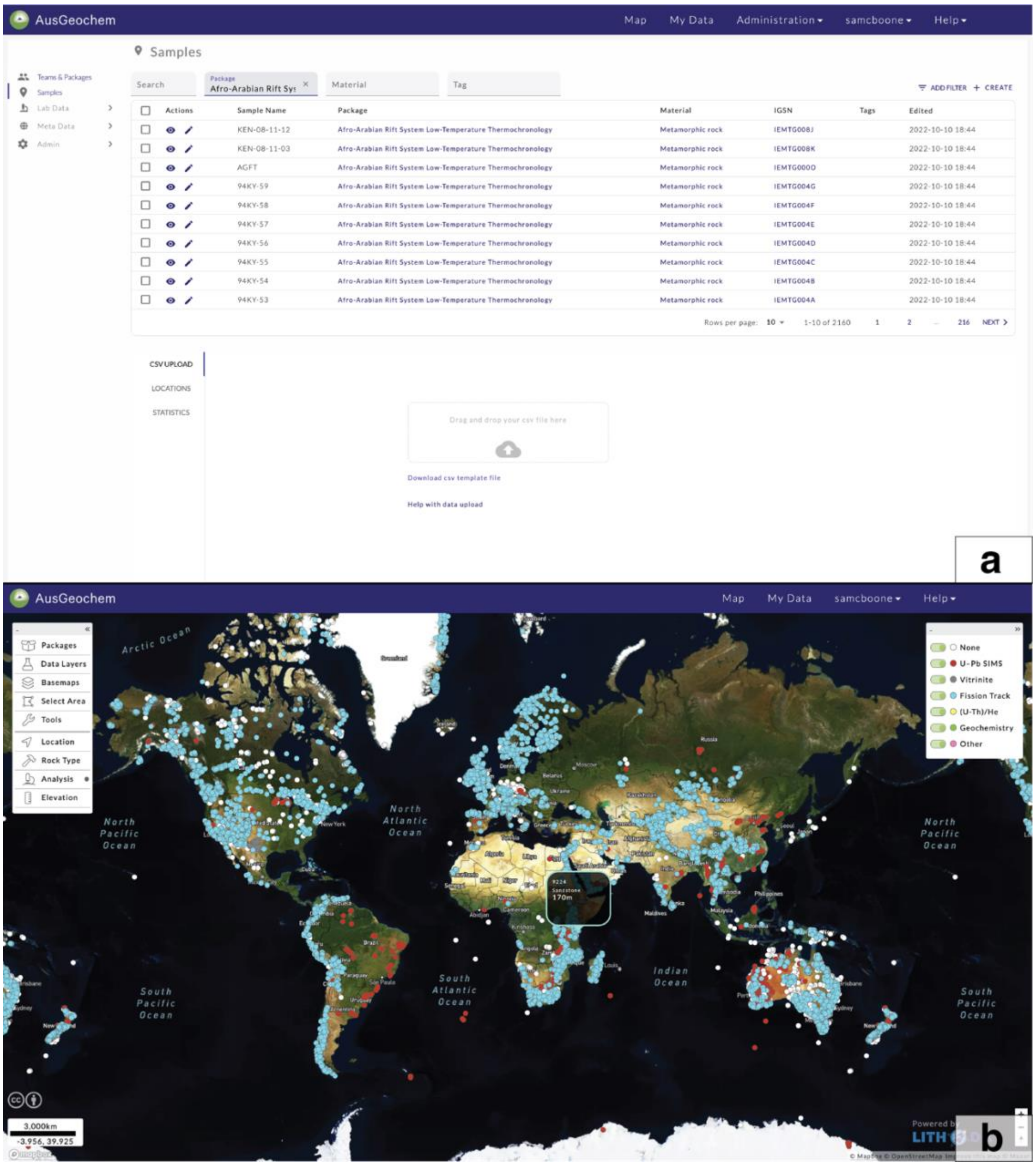

Fig. 2. AusGeochem user interface. (A) My Data interface. **(B)** Map View interface. Displayed data (selected by Data Package), data types, basemaps, a choice of data search tools, and a series of filters (location type, rock type, analytical method, elevation) can be selected from the toolbar on the left-hand side.

Data Management

Fission-track and (U-Th)/He data management is performed in the My Data section of *AusGeochem* (*44*), where users can upload and edit analyses individually or in bulk via a drag-and-drop tool using .csv or .xlsx data templates downloadable from within the platform. For efficient data uploading, single-grain fission-track count data and length measurements obtained using the digital fission-track analysis software *FastTracks* (*48*) can be rapidly uploaded into *AusGeochem* using the 'AusGeochem Count Data' and 'AusGeochem Length Data' export formats available in *FastTracks* (version 3.3.5 and above), which can be dropped directly into the bulk upload boxes on the respective My Data tabs.

In addition to uploading analyses of unknowns, AusGeochem users are also highly encouraged to archive associated secondary reference material results. This is critical as it allows platform users to independently assess data quality based on the reproducibility of well-characterised reference materials of known composition and/or age. For fission-track analysis, this or for absolute age determinations via LA-ICP-MS or EPMA. Once uploaded, the associated reference material results for a given unknown analysis can then be quickly viewed under the Analytical Data pop-up when that sample is selected in Map View (Fig. 3).

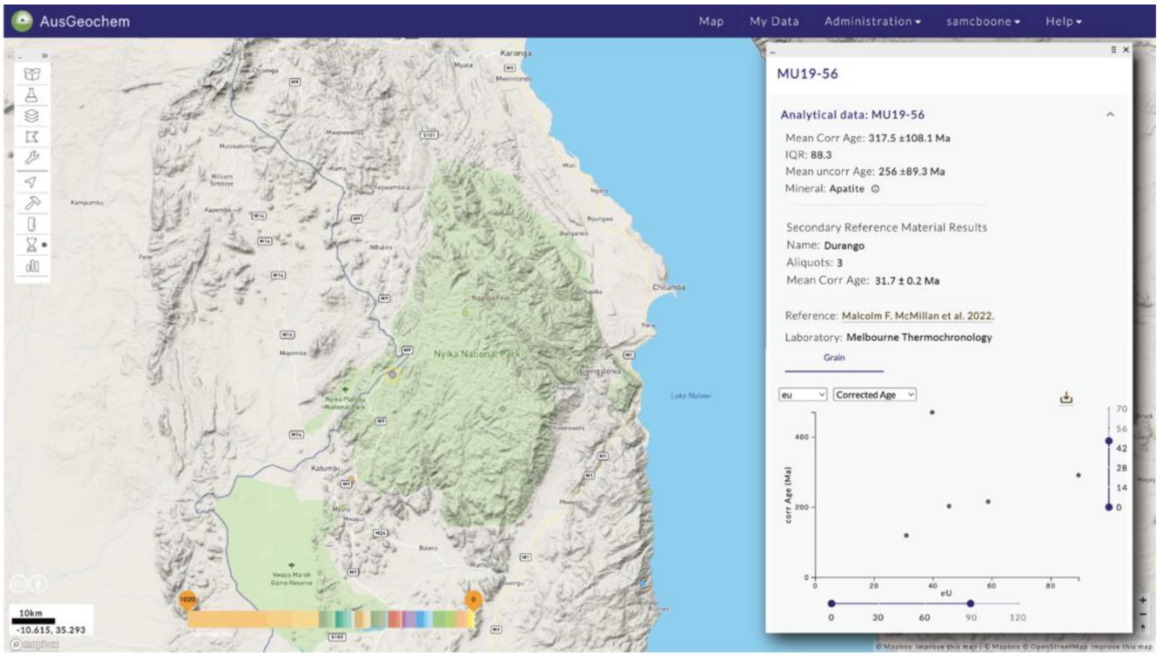

Fig. 3. Sample metadata, analytical results, and associated secondary reference material results in the AusGeochem Map View. Unknown and secondary reference material results are related to one another via their Batch ID, a unique identifier corresponding to results obtained as part of the same set of data acquisition, allowing for rapid data quality assessment. Apatite (U-Th)/He data from McMillan et al. (*49*).

Selected data can be extracted from both Map View and My Data, and exported in .csv and .xlsx formats. Users are also encouraged to code their own routines for streamlined fission-track and (U-Th)/He data upload and download directly to and from third-party software, repositories, or databases using *AusGeochem's* open REST API (see below).

Data Interrogation in Map View

AusGeochem's Map View user interface enables geological sample and geochemistry data to be explored in their geospatial context. Users can select data types and perform further data filtering in Map View using a combination of lithological, mineralogical, elevation, and method-specific attributes (Fig. 2b).

A selection of base maps and map projections are available, including satellite images, dark and light contrast maps, topography, and global geology, all of which can be viewed in a Web Mercator (EPSG:900913) or spherical projection (Fig. 4). Where available, other regional base maps, such as regional gravity, magnetic, and heat-producing radioactive elemental concentration data layers can also be viewed (Fig. 4c). Data can also be viewed in their 3D topographical context. In this way, any base map layer can be draped over the vertically exaggerated digital elevation model (e.g., geology, Fig. 4d).

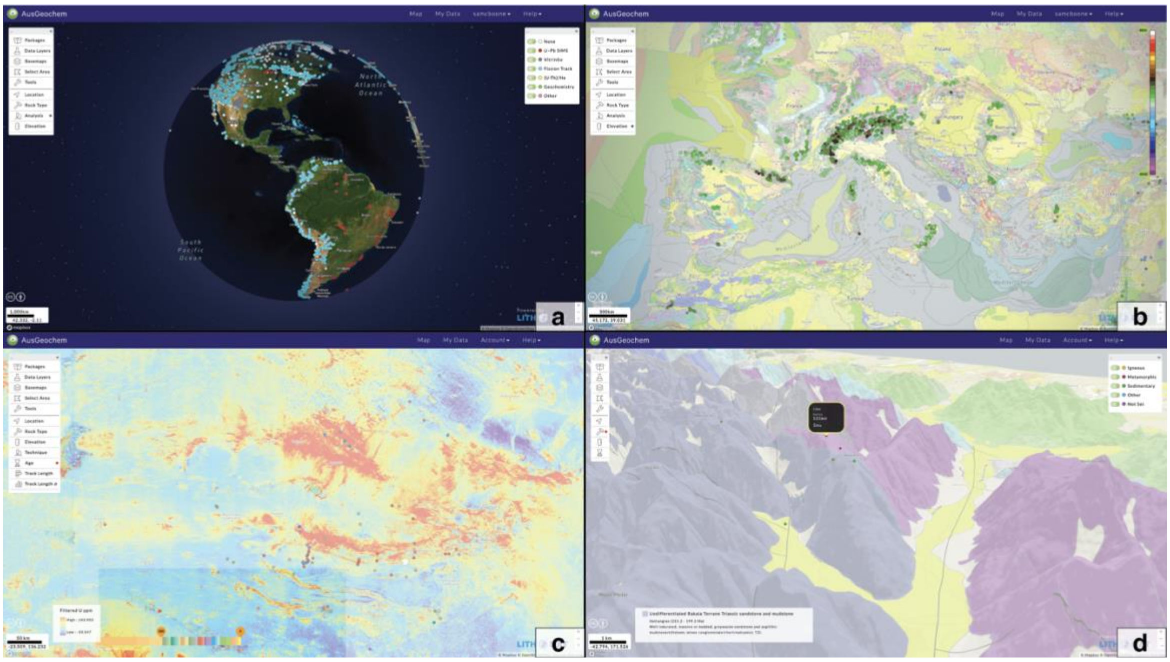

Fig. 4. A range of base maps and data projections in AusGeochem. (A) samples coloured by data type on a satellite image base map in spherical projection, **(B)** samples coloured by elevation on geological base map, **(C)** fission-track data (*50*) by age on gravity anomaly map, **(D)** and 3D perspective of apatite (U-Th)/He data by rock type on geological map.

Simple sample and analytical information can be retrieved via a pop-up window by hovering the cursor over a sample point on the map (Fig. 2b), while more detailed (meta-)data can be obtained by selecting a given sample (Fig. 3). A range of data interrogation tools are also available. These include a data interpolation tool, which generates contoured heat maps for selected variables like age or mean track length (Fig. 5a) and a swath profile tool for investigating the relationship between selected attributes and topography (Fig. 5b). Using the Multi-Select tool, numerous samples on the map can be selected simultaneously allowing for real-time data synthesis and visualisation. By dragging a polygon over an area of interest, a simplified table summarising the selected data points can be queried. Here, users can then select from a range of method-specific dashboards (Fig. 6) which synthesise the selected data in real-time via comparative plots and derivative maps relevant for each methodology.

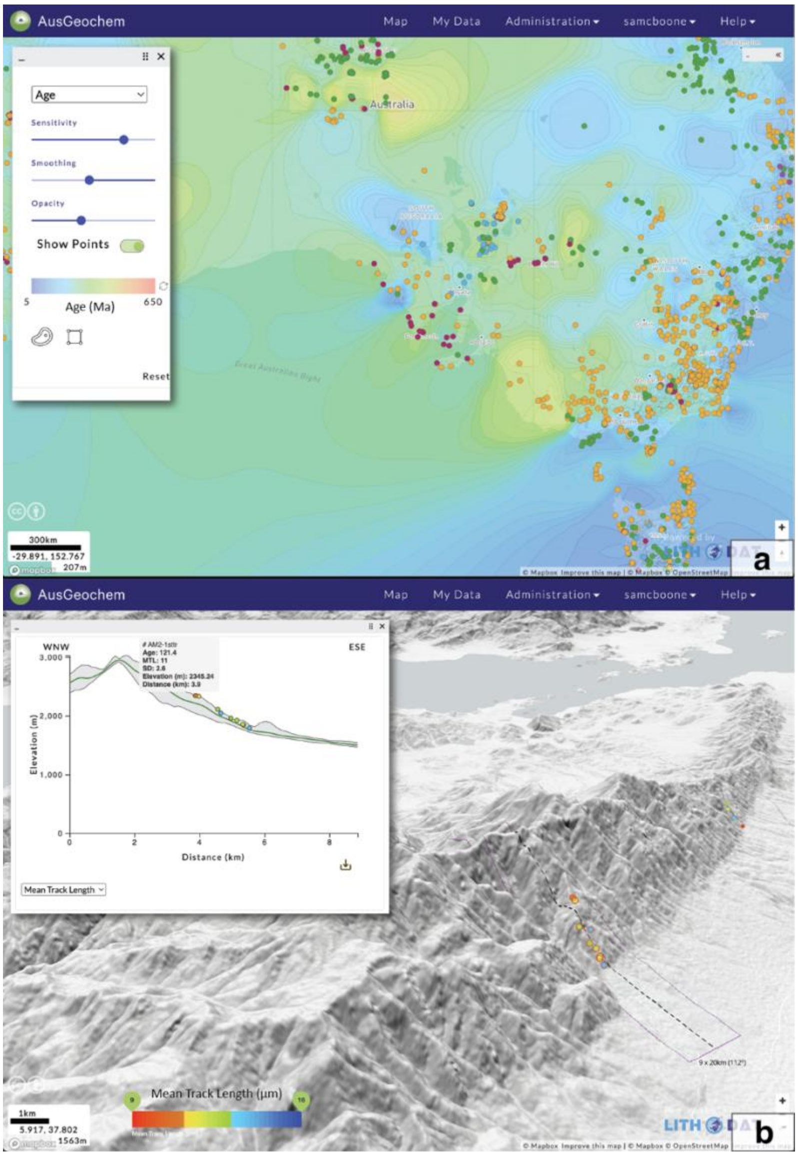

Fig. 5. Data interrogation tools in AusGeochem. (A) Data interpolation tool, contouring apatite fission-track ages in southern Australia (*50*). **(B)** Swath profile tool, illustrating the relationship between apatite fission-track mean track lengths and topography in a vertical profile in the margin of the Galana rift basin of Ethiopia (*51*).

Fission-Track and (U-Th)/He Dashboards

The bespoke fission-track and (U-Th)/He dashboard provides users with intuitive tools to interrogate select collations of thermochronology data via a range of maps, tables, and interactive plots (Fig. 6), all of which can be exported in publication ready formats. Dashboard plots include an age histogram, radial plot, boomerang plot, age versus elevation plot, and flexible scatterplots that allows users to plot fission-track ages versus any geochemical parameter, all of which can be downloaded as .svg files for further editing if needed. To ensure that data producers are appropriately credited, the dashboards also provide a downloadable reference list associated with the selected data (Fig. 6).

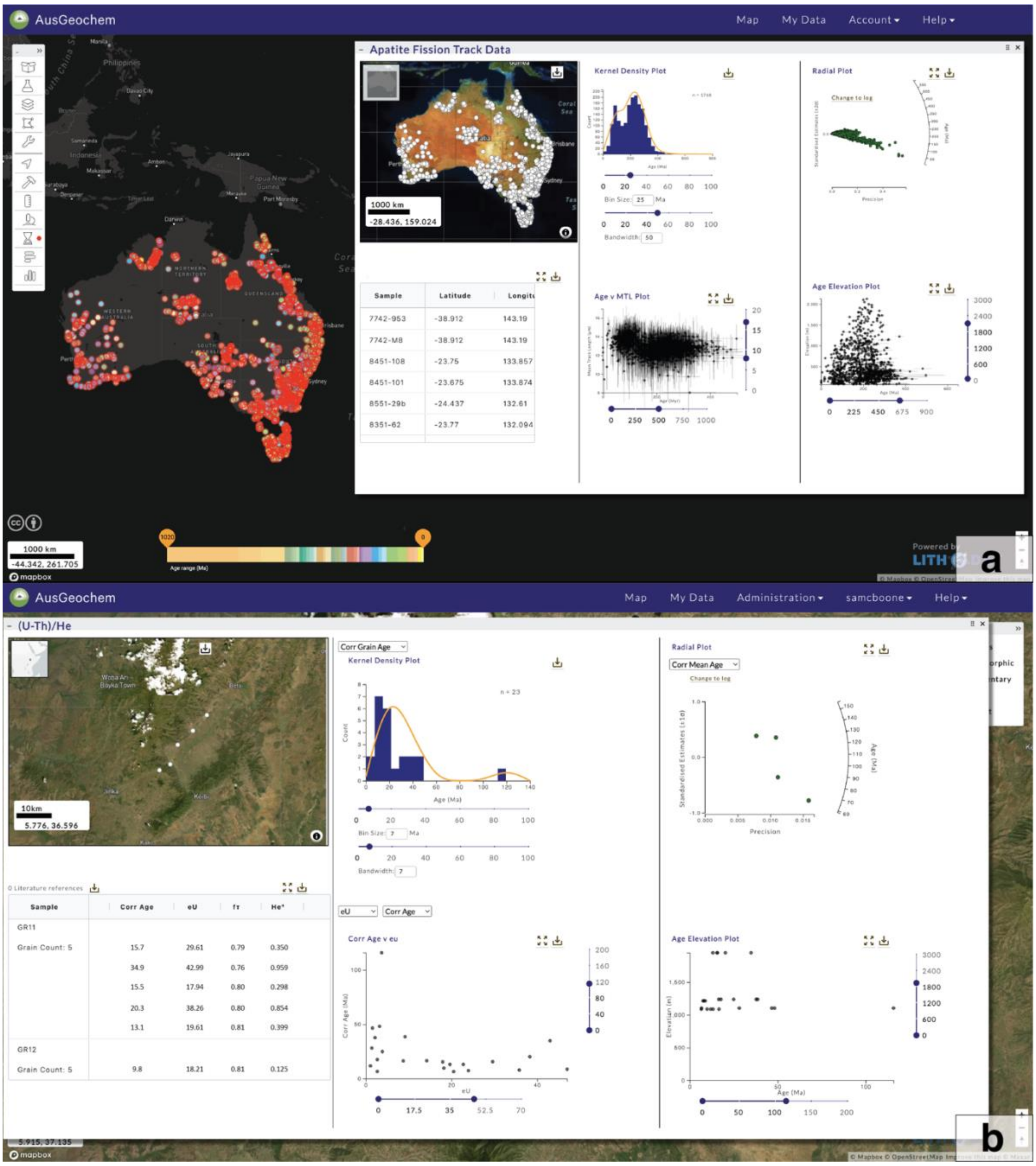

Fig. 6. The AusGeochem fission-track (A) and (U-Th)/He (B) dashboards. Dashboards enable multiple data points, chosen using the Select Area tool, to be collectively interrogated via a range of interactive maps, plots and tables. The inset map and all plots can be downloaded as editable svg files. A succinct data table can also be downloaded as a csv file. A downloadable reference list for all selected data points is also automatically generated, ensuring data sources can be appropriately cited. Apatite fission-track data **(A)** were sourced from Gleadow et al. (*50*), while apatite (U-Th)/He data **(B)** were sourced from Boone et al. (*51*).

Application Programming Interface (API)

AusGeochem is equipped with an Open REST API, allowing any developer to build clients that can interact with the platform to, for example, automatically upload or retrieve data from its database, add enhanced data visualisation tools and create direct links to analytical equipment. Potential uses of this powerful tool for the low-temperature thermochronology community could include the development of clients enabling automated data upload using common data formats (e.g., TrackKey, *42*; HeFTy, *43*; or QTQt files, *52*) and automated data retrieval for bulk thermal history modelling or landscape evolution modelling (e.g., with Pecube, *53*).

API documentation and user instructions on how to access the API can be found under the Help tab in *AusGeochem*.

Discussion

The relational fission-track and (U-Th)/He data models of *AusGeochem* provide novel tools for dynamic geospatial interrogation of low-temperature thermochronology data. To illustrate this, three regional case studies from around the globe are briefly presented below. Through these examples, the importance of interrogating large compilations of fission-track and (U-Th)/He data in their geospatial context is demonstrated using the built-in tools currently available within *AusGeochem*. While these examples highlight regional fission-track and (U-Th)/He methods applications in intracontinental rifting, continental breakup, and passive margin settings, it is stressed that *AusGeochem* is designed to geospatially interrogate low-temperature thermochronology data at all scales, across the full breadth of geological environments. The case studies are followed by a discussion of potential future developments and powerful applications of this relational thermochronology data platform.

Readers can interrogate and utilise the detailed regional fission-track and (U-Th)/He datasets discussed below, which are freely available on *AusGeochem*. Data users are strongly encouraged to cite all data sources and data compilers in line with FAIR data principles (*45*). Reference information for each data point can be found in their metadata under “Literature”.

Thermochronological Imaging of Tectonic Inheritance in Kenya

The East African Rift System (EARS) has long attracted geoscientists looking to employ low-temperature thermochronology to investigate intracontinental rift processes. This has resulted in a dense coverage of low-temperature thermochronology analyses, particularly apatite fission-track data in Kenya (Fig. 7). When viewed regionally in *AusGeochem*, these data reveal the tectonothermal signature of a long history of superimposed tectonic events imprinted into the East African crust. Taken together, these data provide an informative snapshot into the geological processes that have most affected the cooling history of rocks now exposed at the surface, often reflecting the timing and rate of erosional denudation in response to tectonism.

The oldest apatite fission-track dates (204 ± 11 to 364 ± 18 Ma) within Kenya are found in Archean rocks of the Tanzanian Craton and Neoproterozoic mobile belts of central Kenya. While the geological significance of these dates is poorly understood, in part due to a dearth of confined track data collected using modern techniques (Fig. S1), the preservation of these old ages attest to the relative stability of the Tanzanian Craton since the Palaeozoic. The most prominent tectonothermal signature recorded in the region, however, is recorded by a profusion of ~100-50 Ma ages (orange in Fig. 7b) observed in a linear band from southeast to northwest Kenya. These have been interpreted as reflecting >2.5 km of rift shoulder uplift and denudation along the margins of the Anza Rift, a failed Cretaceous-early Paleogene rift system running northwest from the Kenyan coast (*54*) that once may have extended across the Turkana Depression into South Sudan (*55*). Surprisingly, few data yield Neogene cooling ages (red in Fig. 7b) associated with the development of the Miocene-recent Kenyan sector of the EARS, despite the rift dominating the modern geomorphology of the region. This suggests EARS-related rift-shoulder uplift has been insufficient to exhume rocks which have cooled entirely through the temperature sensitivity range of the apatite fission-track system. Only in the Turkana Depression of northern Kenya and localised along a basin-bounding normal fault in central Kenya are Neogene cooling ages recorded, with the former attributed to a combination of higher palaeogeothermal gradients and increased basin margin uplift due to lower flexural rigidity of the highly attenuated crust there (*56*) and the latter associated with localised hydrothermal fluid activity (*57*).

However, some of the most important insights into what governs the low-temperature thermochronology of the upper crust in intracontinental settings can be found when Kenyan apatite fission-track data are juxtaposed against the regional geology (Fig. 7). Despite the surface geology being largely composed of aerially-extensive Neogene volcanic rocks (Fig. 7b), a notable absence of regional thermal rejuvenation of apatite fission-track data by the intense magmatic history of the Kenyan Rift becomes readily apparent. Since the early Miocene, and beginning even earlier (Paleogene) in Turkana, the interplay of plume activity and lithospheric thinning has resulted in the emplacement of a perfuse volume of extrusive volcanic rocks in Kenya (924,000 km^3, *65*) and the addition of unknown, but no doubt significant, amounts of igneous material in the sub-surface (*59*, *60*). Yet, apatite fission-track data yield very few Neogene ages recording the influence of conductive heating related to the extensive magmatic history of the rift. This is consistent with previous assertions that the conductive thermal effect of magmatism on low-temperature thermochronology is restricted to similar length scales of individual lava flow thicknesses and intrusive body dimensions (*1*, *61*, *62*). By readily placing Kenyan thermochronology in its geological context using *AusGeochem*, the utility of regional apatite fission-track assays for constraining the spatio-temporal denudational response to upper crustal extensional strain is demonstrated, even in a magmatic intracontinental rift setting.

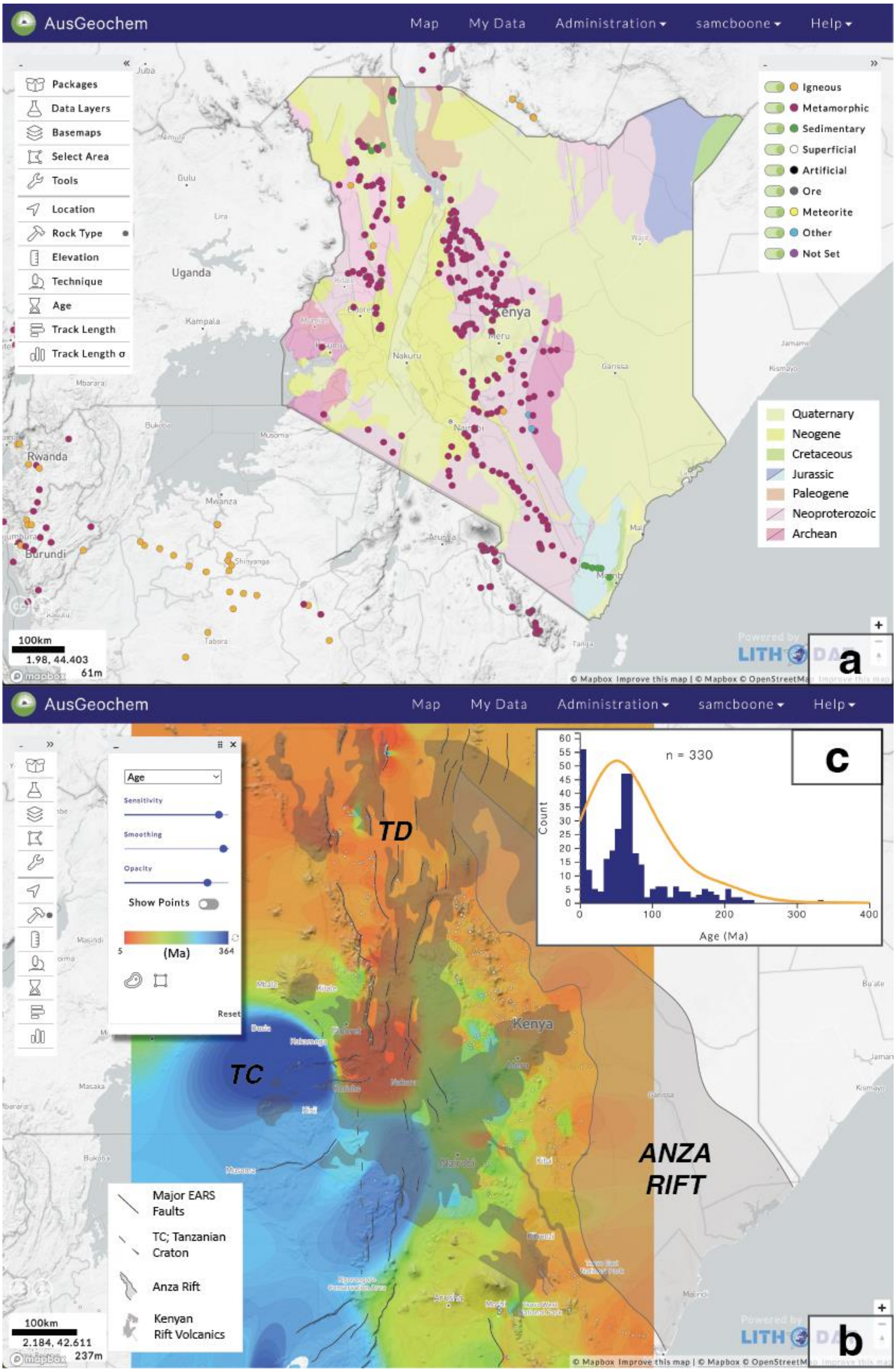

Fig. 7. Simplified geology of Kenya (A), with interpolation (B) and distribution (C) of apatite fission-track ages. Mean track length interpolation and data sources are listed in the Supplementary Material (Fig. S1 & Table S9). All figure elements were exported from AusGeochem before being combined and annotated in a third-party graphics editor program. Distribution of Kenyan rift volcanic rocks from Beicip (*63*). TC = Tanzanian Craton; TD = Turkana Depression; EARS = East African Rift System.

Thermochronological Insights into Australian Passive Margin Evolution

Since Moore et al. (*64*) first reported an apparent relationship between the modern topography of the southeast Australian margin and apatite fission-track data observed along a transect orthogonal to the coast, low-temperature thermochronology has routinely been used to constrain the denudation history of rifted continental margins (*65–67*), leading to the development of a range of tectonic models for passive margin development (*68*, *69*). Specifically, Moore and colleagues (*64*) observed a transition from relatively young apatite fission-track ages and long confined track lengths at the coast, through to moderate ages with short track lengths on the erosional escarpment, and eventually to old ages and long track lengths atop the escarpment, which they collectively attributed to a Late Cretaceous rift-related thermal event that preferentially reset apatite fission-track data along the southeast Australian margin (Fig. 8A & 8B). This concave-up "boomerang trend" observed in the apatite fission-track age versus mean track length data (Fig. 8A) has since become a diagnostic signature of progressive thermal overprinting of an older background thermal history by a younger cooling event (*70*), and frequently applied to interpreting the thermochronology of rifted continental margins around the world (*61*, *62*, *69*, *71*).

However, in light of more regional-scale thermochronology data syntheses and integration with other geological evidence, the underlying assumption that the development of modern topography implicitly relates to the underlying apatite fission-track data has recently been called into question in some instances (*72–74*). Even along the southeast Australian margin where it was first observed, the relationship between fission-track data and modern rift margin topography breaks down when viewed in its regional context (*74*). Instead, north of the original apatite fission-track data transect of Moore et al. (*64*) which fortuitously corresponds with the modern topographic profile of the Australian margin, the "boomerang trend" diverges inland (Figs. 8C & 8D). This requires that the apparent pattern in thermochronology data predates the topographic development of the present Australian margin (*74*), bringing into question the assumed genetic link between low-temperature thermochronology data and the modern topographic expression of rifted continental margins worldwide. While not claiming that this re-interpretation may necessarily apply to passive rifted margins elsewhere, it does act as a cautionary tale, encouraging the scrutiny of low-temperature thermochronology datasets from other passive margins in their regional context, which can be readily enabled using the *AusGeochem* platform.

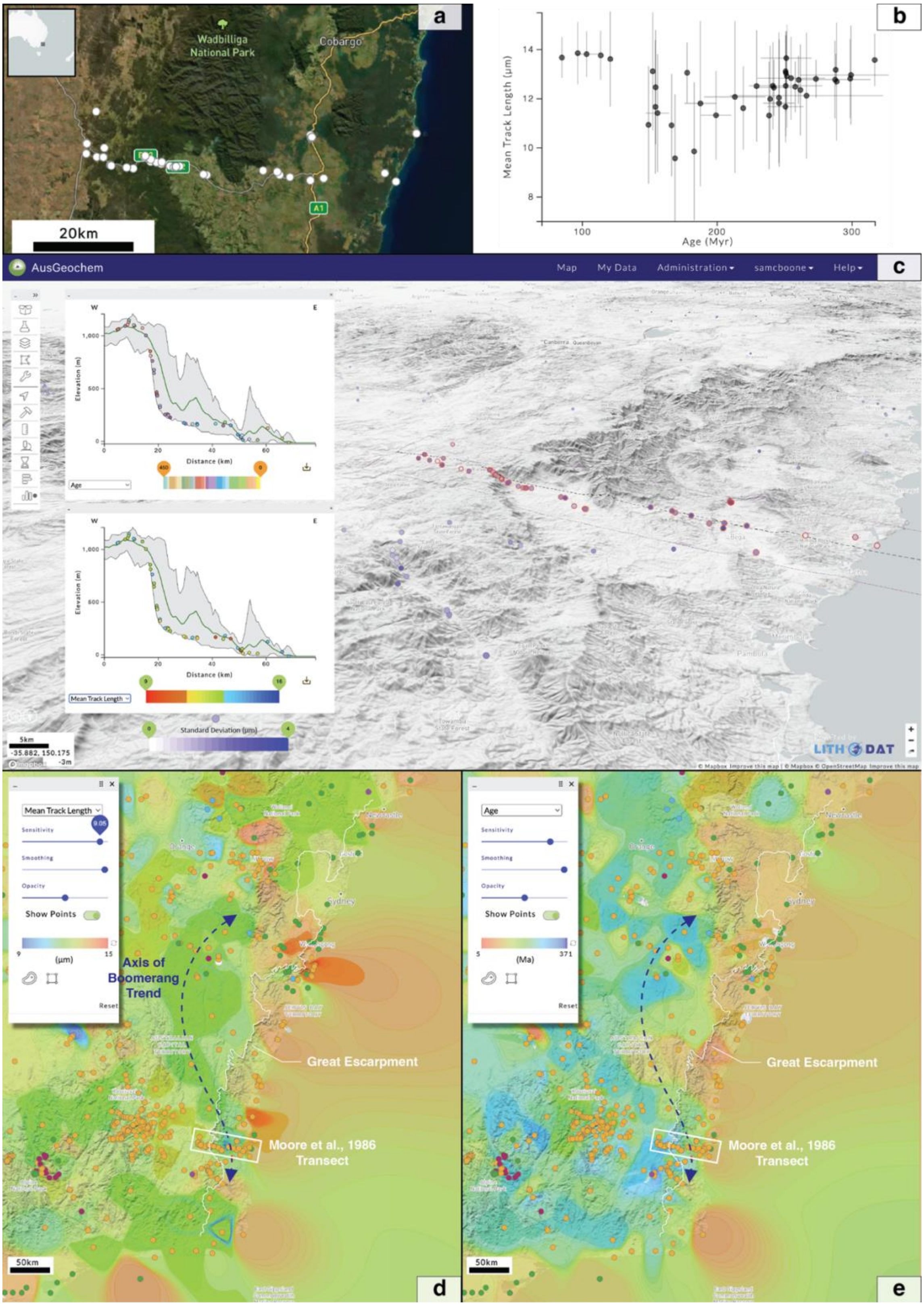

Fig. 8. Apatite fission-track data trends along the eastern Australian margin. (A) Sample locations and **(B)** age versus mean track length (Boomerang) plot of fission-track transect of Moore et al. (*64*) and McMillan et al. (*74*). **(C)** Swath profiles of combined apatite fission-track data transect of Moore et al. (*64*) and McMillan et al. (*74*) showing relationship between age, mean track length, and standard deviation. Regional interpolation of mean track lengths **(D)** and apatite fission-track ages **(E)** from southeast Australia (*50*, *64*, *74*) show how the fortuitous relationship between apatite fission-track data and modern topographic expression of the rifted Great Escarpment breaks down north of the classic transect of Moore et al. (*64*). All figure elements were exported from AusGeochem before being combined and annotated in a third-party graphics editor program.

Geomorphological Evolution of the Red Sea Rift Escarpments

While the development of elevated topography along many modern passive margins may significantly post-date continental breakup (*73*), in some instances long-term denudation rates estimated from low-temperature thermochronology can still provide important constraints for the geomorphic evolution of rifted margins (*69*). Such is the case for the conjugate Nubian-Arabian margins, whose transformation from being topographically subdued in the Early Oligocene to displaying its modern steep coastal escarpments is attributed to the development of the Red Sea rift system since the Late Oligocene (*75*).

Despite an uneven distribution of low-temperature thermochronology data along the Red Sea, marked differences in apatite fission-track (Fig. 9) and (U-Th)/He (Fig. 10) data trends from the Nubian and Arabian margins reflect their disparate geomorphologies (*76*), as clearly shown when viewed in *AusGeochem*. The Nubian margin, whose low-lying deserts are separated from the coast by the narrow Red Sea Hills (500 m mean elevation), contrasts starkly with the broad highlands (1,000-1,500 m mean elevation) of the Arabian margin that attains heights of up to 3,200 m at its southern end. This physiographic asymmetry is reflected in the low-temperature thermochronology data. Whereas the Arabian margin yields Oligo-Miocene apatite fission-track and (U-Th)/He ages and long mean track lengths along the full extent of its rift escarpment, indicative of rapid exhumation during that time period, the Nubian margin exhibits significantly older thermochronological ages along most of its topographically subdued profile. Pronounced Miocene cooling is observed only at the southern extent of the Nubian margin along the base of the >2,000 m Ethiopian Plateau is pronounced Miocene cooling observed, where its tectonothermal evolution related to the opening of the southern Red Sea is compounded by additional plume activity and incipient lithospheric rupture in the Afar (*77*). Debate continues as to why the conjugate margins of the Red Sea rift evolved so differently (*78*), with explanations ranging from northeast tilting of Arabia due to its collision with Eurasia (*79*) to dynamic topography gradients (*80*). Nevertheless, the pronounced differences in the timing and rate of rift margin uplift quantified by low-temperature thermochronology provide valuable observations with which to test these geodynamic hypotheses.

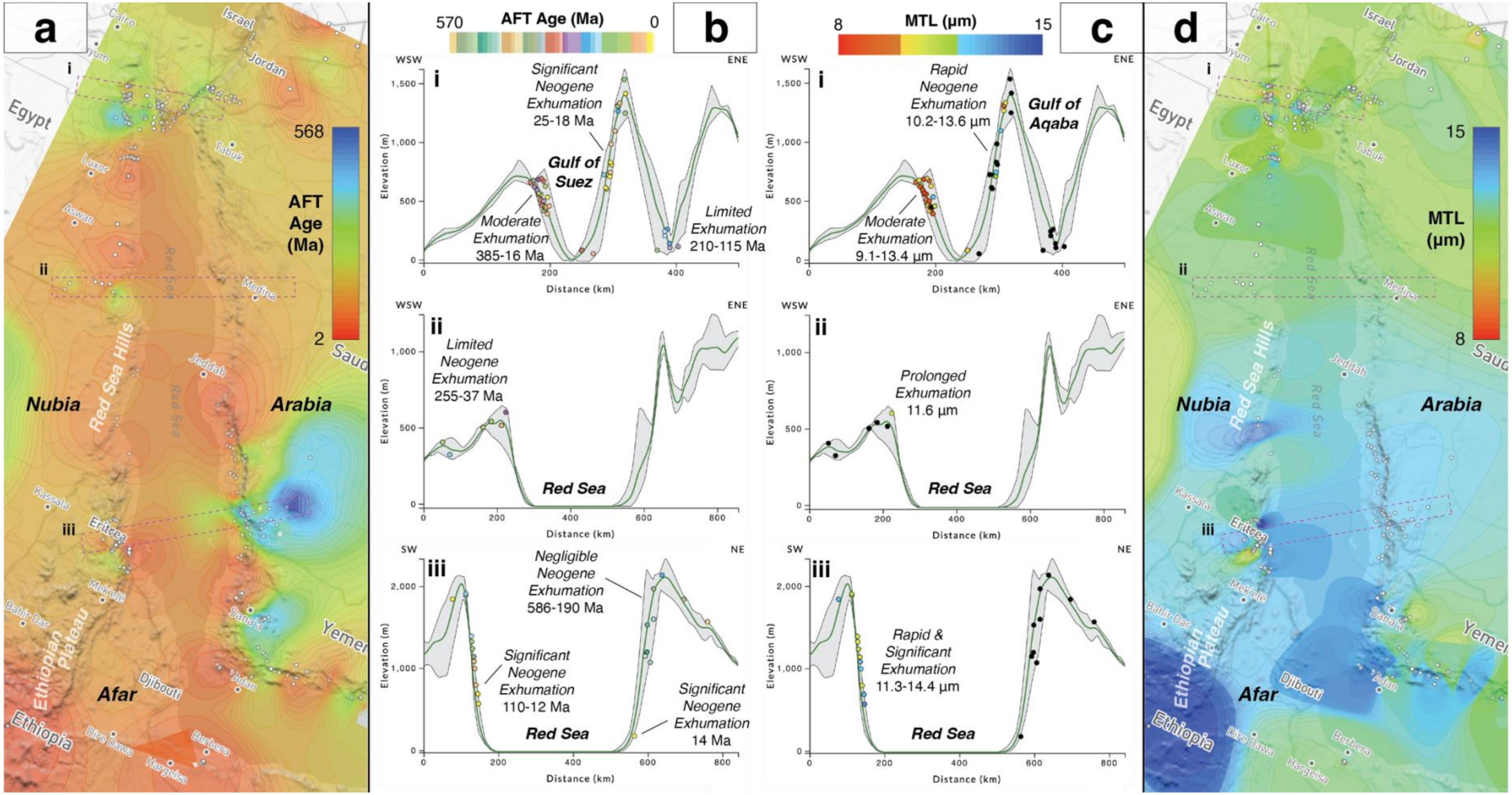

Fig. 9. Relationship between apatite fission-track data and geomorphology along the Red Sea Margins. Data sources are listed in the Supplementary Materials (Table S10). (**a, b**) Fission-track age and (**c, d**) mean track length (MTL) interpolations and swath profiles were exported from AusGeochem before being annotated in a third-party graphics editor program. Black dots in swath profiles indicate no data.

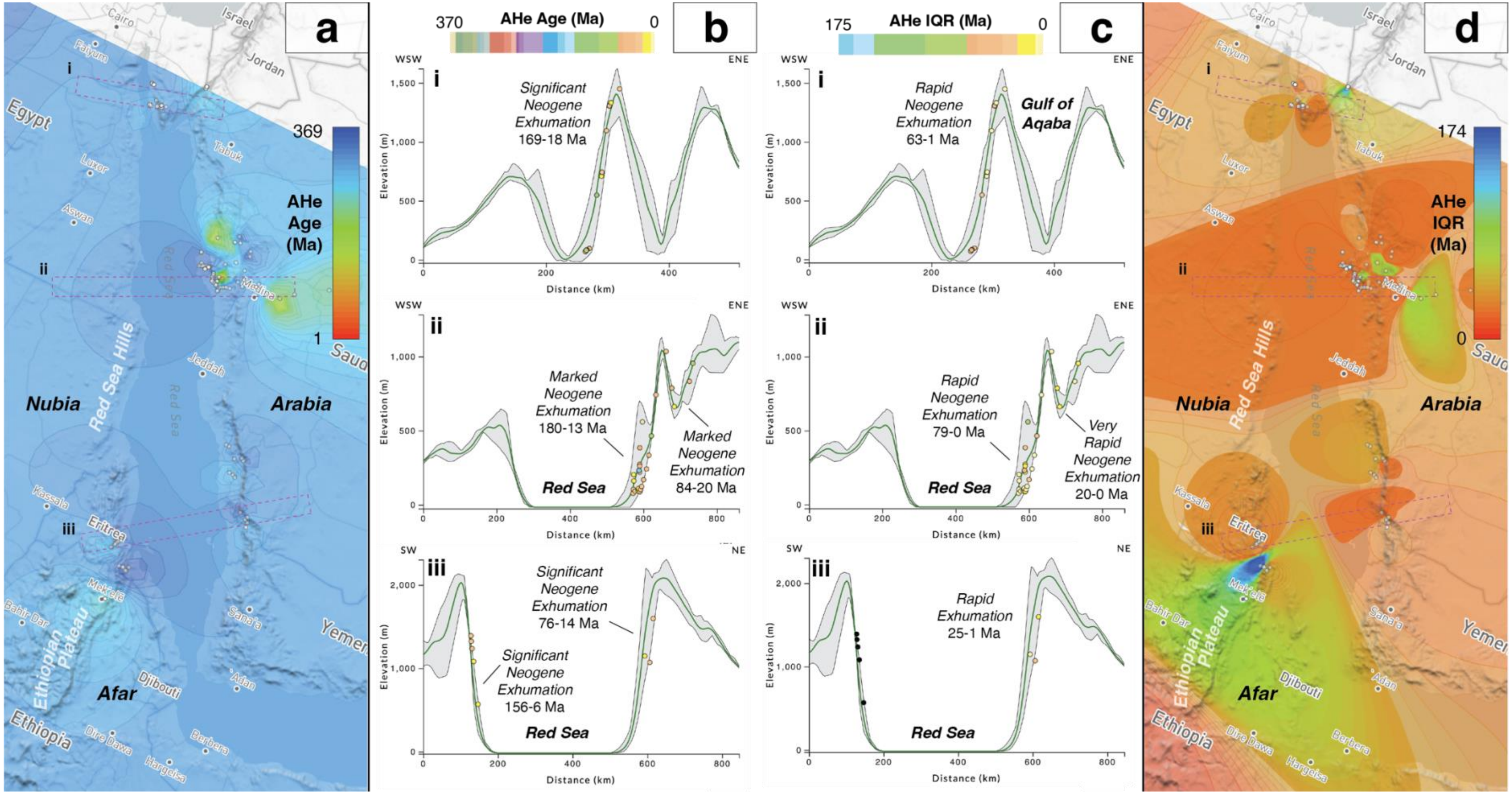

Fig. 10. Relationship between apatite (U-Th)/He data and geomorphology along the Red Sea Margins. Data sources are listed in the Supplementary Materials (Table S10). (**a, b**) Mean apatite (U-Th)/He age and (**c, d**) interquartile range (IQR) interpolations and swath profiles were exported from AusGeochem before being annotated in a third-party graphics editor program. Black dots in swath profiles indicate no data.

Future Outlook

The advent of dynamic relational fission-track and (U-Th)/He databases heralds the beginning of a new era of structured Big Data in the field of low-temperature thermochronology. By methodically archiving detailed fission-track and (U-Th)/He (meta-)data in structured schemas, intractably large datasets comprising 1000s of analyses produced by numerous laboratories from around the globe can be readily interrogated in new and powerful ways. The collective use of a single community-designed data reporting schema will also aid the low-temperature thermochronology community to converge on more consistent data reporting practices, better connecting data producers and users. The ability to geospatially search available fission-track and (U-Th)/He data and immediately access all of the associated detailed analyses will make data mining significantly more time efficient, while also providing a means to rapidly identify data gaps for future research.

Yet, the ability to rapidly visualise and synthesise fission-track and (U-Th)/He analyses in a geospatial context is but a hint at the true potential of archiving low-temperature thermochronology data in a structured database architecture. With detailed thermochronology data stored in relational schemas, the step to developing scripts capable of re-calculating and re-modelling analyses using user-defined constants and kinetic algorithms is relatively straightforward. Such a future advancement would enable analyses determined using different parameters and constants to be equated and compared across regional- to global scales. Similarly, *AusGeochem's* open API could be leveraged to automate thermal history modelling of thousands of samples on a regional scale, retrieve large collections of data for numerical landscape evolution modelling, or place fission-track analyses in palinspastic and/or paleoclimactic reconstructions.

Readers may freely register and explore *AusGeochem* and its low-temperature thermochronology data tool at https://ausgeochem.auscope.org.au.

Materials and Methods

AusGeochem geochemistry data platform

In 2019, a consortium of Australian university research laboratories named the AuScope Geochemistry Network set out to build a collaborative platform for the express purpose of collating, preserving, and disseminating geochemistry and geochronology data. In partnership with geoscience-data-solutions company Lithodat Pty Ltd, the open, cloud-based *AusGeochem* platform (https://ausgeochem.auscope.org.au, *44*) was developed to simultaneously serve as a geosample registry, a geochemical data repository, and a data interrogation tool. In collaboration with method-specific advisory groups of geochemistry experts and adopting established international data reporting practices, community-agreed upon data schemas have been developed for rock and mineral geosample metadata, secondary ion mass spectrometry U-Pb analysis, fission-track and (U-Th)/He analysis. These will be accompanied progressively by additional data models for laser ablation inductively coupled mass spectrometry (LA-ICP-MS) U-Pb and Lu-Hf, oxide and major, minor and trace element geochemistry, and Ar-Ar, all currently under development, with the intention of additional method-specific geochemistry data models to follow.

Fission-track and (U-Th)/He database scope and development

Schemas for the *AusGeochem* fission-track data model (Tables S1-S5) and (U-Th)/He data model (Tables S6-S8) were designed with the aim of accommodating retrospective and prospective datasets alike. Such flexibility requires that the data schema can archive analyses produced across mineral systems and via the breadth of historical fission-track and (U-Th)/He techniques. For the fission-track system, this includes results generated from the outdated population method (*81*), conventional external detector method (EDM, e.g., *32*), and state-of-the-art in-situ fission track analysis using laser ablation inductively coupled plasma mass spectrometry (LA-ICP-MS, e.g., *89*, *90*) or electron probe microanalysis (EPMA), in the case of analysis of relatively U-rich mineral assemblages like zircon (*84*). For the (U-Th)/He system, the current version of the (U-Th)/He relational data model is built to accommodate whole-grain and in-situ age determinations. While the current *AusGeochem* (U-Th)/He relational data model cannot accommodate results generated via the emerging $^{4}He/^{3}He$ or Continuous Ramped Heating methods (*29*), its flexible architecture would allow for straightforward integration of bespoke data tables for these analysis types, should they be designed in the future (Fig. 1).

The relational FT database was also designed to handle wildly varying degrees of (meta-)data reporting granularity found across the gamut of published thermochronology studies. So, in addition to archiving whole-rock fission-track results (Table S1), the model can accommodate both detailed single-grain fission-track count (Table S3) and age data (Table S2), when available. Similarly, users are able to upload both comprehensive confined fission-track length data (Table S4) generated using digital microscopy software (e.g., *FastTracks*, *48*), or legacy binned confined track data reported simply as length histograms without the corresponding detailed length parameters (Table S5). While the fission-track model is strictly designed to accommodate fission-track analyses sensu stricto, associated in-situ geochemical analyses obtained via EPMA or LA-ICP-MS trace element analysis can be archived and related to fission-track results on a per-sample, per-grain, and per-spot basis in the linked Major, Minor and Trace Element Geochemistry Data Model (Fig. 1).

The (meta-)data fields and corresponding units of the fission-track and (U-Th)/He data tables were designed after global community-agreed reporting recommendations. The (U-Th)/He data model and corresponding tables (Tables S6-S8) were designed following the data reporting best-practices of Flowers et al. (*29*). While the fission-track model (Tables S1-S5) was designed after the recommended data reporting practices currently being prepared for submission to *Geological Society of America Bulletin* special edition on "Reporting and Interpretation of Fission-Track Chronology Data", with which co-authors of this article (B.K, S.B., A.G., and M.D.) are involved.

<u>AusGeochem data platform architecture</u>

The fission-track and (U-Th)/He data models presented herein were designed as an extension to the *AusGeochem* (*44*) relational database architecture (Fig.1). The *AusGeochem* platform comprises four integral components. At the highest level is the Model for Management, which enables users to manage data privacy control on a per dataset basis, called 'Data Packages' in *AusGeochem*. Upon data upload, users have the option to keep their unpublished data private, disseminate their data to select collaborators, or make their data open access. This user-defined privacy control system gives analysts the ability to upload and interrogate their unpublished data in the context of thousands of results from around the globe, whilst keeping their data private until results are ready for publication. However, uploaded data is subject to *AusGeochem's* open data policy, which limits the data privacy embargo to two years plus the option for an automatic 1-year privacy extension.

Geological mineral and rock samples, along with their associated information, are stored in the Core Model. From here, samples can be linked to Method-Specific analyses, such as those stored in the fission-track or (U-Th)/He data models. Each sample can have multiple related method-specific Data Points, each of which represents a particular analysis performed on that geosample. In other words, an individual sample can be linked to multiple analyses, such that the reanalysis of a given sample would simply be uploaded as a new method-specific Data Point (e.g., an FT Data Point). This 1-n relationship between the Core Model and the Method-Specific Models also allows geochemical data of different kinds to be related on a per-sample or per-aliquot basis. This is particularly relevant for fission-track analyses which are often accompanied by other complementary geochemical measurements. For example, fission track results can be linked to corresponding electron probe microanalysis, LA-ICP-MS trace element, and U-Pb data stored in other Method-Specific Data Models via their shared Sample, Mount, Grain, and in some cases, Spot IDs (Fig. 1). Thus, *AusGeochem* will also be able to accommodate the archival of double- and triple-dating results involving combined fission-track, U-Pb, and (U-Th)/He determinations (*83*, *85*, *86*).

The fourth component of the *AusGeochem* platform is the Statement Model, which enables advanced on-the-fly analytics to be performed across all Data Points and data types. Here, the 'statement(s)' derived for each Data Point, such as age, chemistry, isotopic ratio, or time-temperature history, are stored.

Acknowledgments

Funding:

This work was enabled by AuScope and the Australian Government via the National Collaboration Research Infrastructure Strategy (NCRIS): auscope.org.au.
SG is supported by an Australian Research Council Future Fellowship (FT210100906).

Author contributions:
Tool conceptualization and design: SB, FK, WN, MT, RB
Back-end programming: MT
Front-end programming: WN
Project supervision: AG, BM
Relational database design: SB, FK, BK, SG, MD, RZ
Visualization and analytical tool design: SB, FK, WN
Platform testing: SB, FK, WN, MM, AN
Writing—original draft: SB
Writing—feedback: FK, MT, BK, SG, MD, RZ, MM, AN

Competing interests:
Authors declare that they have no competing interests.

Data and materials availability:
The *AusGeochem* data platform and the low-temperature thermochronology data extension presented here are open-access and freely available to users from around the world at https://ausgeochem.auscope.org.au. Relational fission-track and (U-Th)/He data tables, including descriptions and units of all attribute fields are available in the main text or the supplementary materials. API documentation and user instructions on how to access the open REST Application Programming Interface (API) can be found under the Help tab in *AusGeochem*.

References

1. T. a. Ehlers, Crustal Thermal Processes and the Interpretation of Thermochronometer Data. *Rev. Mineral. Geochemistry*. **58**, 315–350 (2005).

2. D. F. Stockli, Application of low-temperature thermochronology to extensional tectonic settings. *Rev. Mineral. Geochemistry*. **58**, 411–448 (2005).
3. P. W. Reiners, M. T. Brandon, Using Thermochronology to Understand Orogenic Erosion. *Annu. Rev. Earth Planet. Sci.* **34**, 419–466 (2006).
4. T. F. Schildgen, P. A. van der Beek, *The Application of Low-Temperature Thermochronology to the Geomorphology of Orogenic Systems* (Springer International Publishing, 2019; http://dx.doi.org/10.1007/978-3-319-89421-8_19).
5. A. K. Ault, C. Gautheron, G. E. King, Innovations in (U–Th)/He, Fission Track, and Trapped Charge Thermochronometry with Applications to Earthquakes, Weathering, Surface-Mantle Connections, and the Growth and Decay of Mountains. *Tectonics*. **38**, 3705–3739 (2019).
6. B. P. Kohn, B. Pillans, M. S. McGlone, Zircon fission track age for middle Pleistocene Rangitawa Tephra, New Zealand: stratigraphic and paleoclimatic significance. *Palaeogeogr. Palaeoclimatol. Palaeoecol.* **95**, 73–94 (1992).
7. P. Shane, P. Froggatt, T. Black, J. Westgate, Chronology of Pliocene and Quaternary bioevents and climatic events from fission-track ages on tephra beds, Wairarapa, New Zealand. *Earth Planet. Sci. Lett.* **130**, 141–154 (1995).
8. H. B. D. Miller, P. M. Vasconcelos, J. M. Eiler, K. A. Farley, A Cenozoic terrestrial paleoclimate record from He dating and stable isotope geochemistry of goethites from Western Australia. *Geology*. **45**, 895–898 (2017).
9. C. Spiegel, B. P. Kohn, D. X. Belton, A. J. W. Gleadow, Morphotectonic evolution of the central Kenya rift flanks: Implications for late Cenozoic environmental change in East Africa. *Geology*. **35**, 427–430 (2007).
10. F. Herman, D. Seward, P. G. Valla, A. Carter, B. Kohn, S. D. Willett, T. A. Ehlers, Worldwide acceleration of mountain erosion under a cooling climate. *Nature*. **504**, 423–426 (2013).
11. D. A. Schneider, D. R. Issler, "Application of low-temperature thermochronology to hydrocarbon exploration" in *Fission-Track Thermochronology and its Application to Geology* (Springer, 2019), pp. 315–333.
12. A. L. Nixon, S. Glorie, D. Hasterok, A. S. Collins, N. Fernie, G. Fraser, Low-temperature thermal history of the McArthur Basin: Influence of the Cambrian Kalkarindji Large Igneous Province on hydrocarbon maturation. *Basin Res.*, 1–24 (2022).
13. B. I. A. McInnes, N. J. Evans, F. Q. Fu, S. Garwin, Application of thermochronology to hydrothermal ore deposits. *Rev. Mineral. Geochemistry*. **58**, 467–498 (2005).
14. S. Glorie, J. W. Hall, A. Nixon, A. S. Collins, A. Reid, Carboniferous fault reactivation at the northern margin of the metal-rich Gawler Craton (South Australia): Implications for ore deposit exhumation and preservation. *Ore Geol. Rev.* **115**, 103193 (2019).
15. L. Gong, B. P. Kohn, Z. Zhang, B. Xiao, L. Wu, H. Chen, Exhumation and preservation of paleozoic porphyry cu deposits: Insights from the yandong deposit, southern central asian orogenic belt. *Econ. Geol.* **116**, 607–628 (2021).
16. Y. Sun, B. P. Kohn, S. C. Boone, D. Wang, K. Wang, Burial and exhumation history of the Lujing uranium ore field, Zhuguangshan, South China: Evidence from low-temperature thermochronology. *Minerals* (2021).
17. K. E. Gorynski, J. D. Walker, D. F. Stockli, A. Sabin, Apatite (U-Th)/He thermochronometry as an innovative geothermal exploration tool: A case study from the southern Wassuk Range, Nevada. *J. Volcanol. Geotherm. Res.* **270**, 99–114 (2014).
18. G. Milesi, P. Monié, P. Münch, R. Soliva, A. Taillefer, O. Bruguier, M. Bellanger, M. Bonno, C. Martin, Tracking geothermal anomalies along a crustal fault using (U-Th)ĝ•He apatite thermochronology and rare-earth element (REE) analyses: The example of the Têt fault (Pyrenees, France). *Solid Earth*. **11**, 1747–1771 (2020).

19. T. Tagami, C. Shimada, Natural long-term annealing of the zircon fission track system around a granitic pluton. *J. Geophys. Res. Solid Earth*. **101**, 8245–8255 (1996).
20. M. Danišík, P. Shane, A. K. Schmitt, A. Hogg, G. M. Santos, S. Storm, N. J. Evans, L. Keith Fifield, J. M. Lindsay, Re-anchoring the late Pleistocene tephrochronology of New Zealand based on concordant radiocarbon ages and combined 238U/230Th disequilibrium and (U-Th)/He zircon ages. *Earth Planet. Sci. Lett.* **349**–**350**, 240–250 (2012).
21. A. Gleadow, M. Harrison, B. Kohn, R. Lugo-zazueta, D. Phillips, The Fish Canyon Tuff : A new look at an old low-temperature thermochronology standard. *Earth Planet. Sci. Lett.* **424**, 95–108 (2015).
22. D. M. Whipp, T. A. Ehlers, Influence of groundwater flow on thermochronometer-derived exhumation rates in the central Nepalese Himalaya. *Geology*. **35**, 851–854 (2007).
23. S. C. Boone, C. Seiler, A. J. Reid, B. Kohn, A. Gleadow, An Upper Cretaceous paleo-aquifer system in the Eromanga Basin of the central Gawler Craton, South Australia: evidence from apatite fission track thermochronology. *Aust. J. Earth Sci.* **63**, 315–331 (2016).
24. C. Seiler, A. J. W. Gleadow, J. M. Fletcher, B. P. Kohn, Thermal evolution of a sheared continental margin: Insights from the Ballenas transform in Baja California, Mexico. *Earth Planet. Sci. Lett.* **285**, 61–74 (2009).
25. S. G. Mitchell, P. W. Reiners, Influence of wildfires on apatite and zircon (U-Th)/He ages. *Geology*. **31**, 1025–1028 (2003).
26. R. Ganapathy, E. Anders, Ages of calcium-rich achondrites—II. Howardites, nakhlites, and the Angra dos Reis angrite. *Geochim. Cosmochim. Acta*. **33**, 775–787 (1969).
27. R. Fleischer, P. Price, R. Walker, Ion explosion spike mechanism for formation of charged-particle tracks in solids. *J. Appl. Phys.* **36**, 3645–3652 (1965).
28. C. W. Naeser, "Fission-track dating and geologic annealing of fission tracks" in *Lectures in isotope geology* (Springer Berlin Heidelberg, 1979), pp. 154–169.
29. R. M. Flowers, P. K. Zeitler, M. Danišík, P. W. Reiners, C. Gautheron, R. A. Ketcham, J. R. Metcalf, D. F. Stockli, E. Enkelmann, R. W. Brown, (U-Th)/He chronology: Part 1. Data, uncertainty, and reporting. *GSA Bull.*, 1–33 (2022).
30. P. W. Reiners, R. W. Carlson, P. R. Renne, K. M. Cooper, D. E. Granger, N. M. McLean, B. Schoene, *Geochronology and thermochronology* (John Wiley & Sons, 2017).
31. G. Wagner, P. Van den Haute, *Fission-Track Dating* (Kluwer Academic Publishers, Dordrecht, 1992).
32. A. J. W. Gleadow, D. X. Belton, B. P. Kohn, R. W. Brown, Fission track dating of phosphate minerals and the thermochronology of apatite. *Phosphates Geochemical, Geobiol. Mater. Importance*. **48**, 579–630 (2002).
33. J. Barbarand, A. Carter, I. Wood, T. Hurford, Compositional and structural control of fission-track annealing in apatite. *Chem. Geol.* **198**, 107–137 (2003).
34. R. W. Brown, R. Beucher, S. Roper, C. Persano, F. Stuart, P. Fitzgerald, Natural age dispersion arising from the analysis of broken crystals. Part I: Theoretical basis and implications for the apatite (U-Th)/He thermochronometer. *Geochim. Cosmochim. Acta*. **122**, 478–497 (2013).
35. K. A. Farley, "(U-Th)/He Dating: Techniques, Calibrations, and Applications" in *Noble Gases in Geochemistry and Cosmochemistry. Reviews in Mineralogy and Geochemistry. No.47.* (Mineralogical Society of America , Washington, DC, 2002), pp. 819–844.
36. D. L. Shuster, R. M. Flowers, K. A. Farley, The influence of natural radiation damage on helium diffusion kinetics in apatite. *Earth Planet. Sci. Lett.* **249**, 148–161 (2006).
37. W. D. Carlson, R. A. Donelick, R. A. Ketcham, Variability of apatite fission-track annealing kinetics: II. Crystallographic orientation effects. *Am. Mineral.* **84**, 1224–1234 (1999).

38. R. A. Donelick, P. B. O’Sullivan, R. A. Ketcham, Apatite fission-track analysis. *Rev. Mineral. Geochemistry*. **58**, 49–94 (2005).
39. R. A. Ketcham, A. Carter, R. A. Donelick, J. Barbarand, A. J. Hurford, Improved modeling of fission-track annealing in apatite. *Am. Mineral.* **92**, 799–810 (2007).
40. W. R. Guenthner, P. W. Reiners, R. A. Ketcham, L. Nasdala, G. Giester, Helium diffusion in natural zircon: radiation damage, anisotropy, and the interpretation of zircon (U-TH)/He thermochronology. *Am. J. Sci.* **313**, 145–198 (2013).
41. J. Braun, P. van der Beek, G. Batt, *Quantitative thermochronology: numerical methods for the interpretation of thermochronological data* (Cambridge University Press, 2006).
42. R. A. Ketcham, Forward and inverse modeling of low-temperature thermochronometry data. *Rev. Mineral. Geochemistry*. **58**, 275–314 (2005).
43. K. Gallagher, Transdimensional inverse thermal history modeling for quantitative thermochronology. *J. Geophys. Res. Solid Earth*. **117**, 1–16 (2012).
44. S. C. Boone, H. Dalton, A. Prent, F. Kohlmann, M. Theile, Y. Gréau, G. Florin, W. Noble, S. Hodgekiss, B. Ware, D. Phillips, B. Kohn, S. O’Reilly, A. Gleadow, B. McInnes, T. Rawling, AusGeochem: An Open Platform for Geochemical Data Preservation, Dissemination and Synthesis. *Geostand. Geoanalytical Res.* (2022), doi:10.1111/ggr.12419.
45. M. D. Wilkinson, M. Dumontier, Ij. J. Aalbersberg, G. Appleton, M. Axton, A. Baak, N. Blomberg, J. W. Boiten, L. B. da Silva Santos, P. E. Bourne, J. Bouwman, A. J. Brookes, T. Clark, M. Crosas, I. Dillo, O. Dumon, S. Edmunds, C. T. Evelo, R. Finkers, A. Gonzalez-Beltran, A. J. G. Gray, P. Groth, C. Goble, J. S. Grethe, J. Heringa, P. A. C. t Hoen, R. Hooft, T. Kuhn, R. Kok, J. Kok, S. J. Lusher, M. E. Martone, A. Mons, A. L. Packer, B. Persson, P. Rocca-Serra, M. Roos, R. van Schaik, S. A. Sansone, E. Schultes, T. Sengstag, T. Slater, G. Strawn, M. A. Swertz, M. Thompson, J. Van Der Lei, E. Van Mulligen, J. Velterop, A. Waagmeester, P. Wittenburg, K. Wolstencroft, J. Zhao, B. Mons, Comment: The FAIR Guiding Principles for scientific data management and stewardship. *Sci. Data*. **3**, 1–9 (2016).
46. S. Stall, L. Yarmey, J. Cutcher-Gershenfeld, B. Hanson, K. Lehnert, B. Nosek, M. Parsons, E. Robinson, L. Wyborn, *Nature*, in press.
47. T. Sherratt, "From portals to platforms: building new frame works for user engagement" in *LIANZA 2013* (2019), pp. 1–12.
48. A. J. W. Gleadow, S. J. Gleadow, D. X. Belton, B. P. Kohn, M. S. Krochmal, R. W. Brown, Coincidence mapping – a key strategy for the automatic counting of fission tracks in natural minerals. *Geol. Soc. London Spec. Publ. Thermochronological Methods From Palaeotemperature Constraints to Landsc. Evol. Model.* **324**, 25–36 (2009).
49. M. F. McMillan, S. C. Boone, B. P. Kohn, A. J. Gleadow, P. R. Chindandali, Development of the Nyika Plateau, Malawi: A Long Lived Paleo-Surface or a Contemporary Feature of the East African Rift? *Geochemistry, Geophys. Geosystems*. **23** (2022), doi:10.1029/2022GC010390.
50. A. J. W. Gleadow, B. P. Kohn, R. W. Brown, P. B. O’Sullivan, A. Raza, Fission track thermotectonic imaging of the Australian continent. *Tectonophysics*. **349**, 5–21 (2002).
51. S. C. Boone, M. L. Balestrieri, B. P. Kohn, G. Corti, A. J. W. Gleadow, C. Seiler, Tectonothermal Evolution of the Broadly Rifted Zone, Ethiopian Rift. *Tectonics*. **38**, 1070–1100 (2019).
52. I. Dunkl, Trackkey: a Windows program for calculation and graphical presentation of fission track data. *Comput. Geosci.* **28**, 3–12 (2002).
53. J. Braun, Pecube: A new finite-element code to solve the 3D heat transport equation including the effects of a time-varying, finite amplitude surface topography. *Comput. Geosci.* **29**, 787–794 (2003).

54. D. A. Foster, J. W. Gleadow, Structural framework and denudation history of the flanks of the Kenya and Anza Rifts, East Africa. *Tectonics*. **15**, 258–271 (1996).
55. W. Bosworth, Mesozoic and early Tertiary rift tectonics in East Africa. *Tectonophysics*. **209**, 115–137 (1992).
56. S. C. Boone, C. Seiler, B. P. Kohn, A. J. W. Gleadow, D. A. Foster, L. Chung, Influence of Rift Superposition on Lithospheric Response to East African Rift System Extension: Lapur Range, Turkana, Kenya. *Tectonics*. **37**, 182–207 (2018).
57. V. Torres Acosta, A. Bande, E. R. Sobel, M. Parra, T. F. Schildgen, F. Stuart, M. R. Strecker, Cenozoic extension in the Kenya Rift from low-temperature thermochronology: Links to diachronous spatiotemporal evolution of rifting in East Africa. *Tectonics*. **34**, 2367–2386 (2015).
58. D. Latin, M. J. Norry, R. J. E. Tarzey, Magmatism in the gregory rift, East Africa: Evidence for melt generation by a plume. *J. Petrol.* **34**, 1007–1027 (1993).
59. T. O. Rooney, The Cenozoic magmatism of East-Africa: Part I — Flood basalts and pulsed magmatism. *Lithos*. **286**–**287**, 264–301 (2017).
60. T. O. Rooney, The Cenozoic magmatism of East Africa: Part V – Magma sources and processes in the East African Rift. *Lithos*. **360**–**361**, 105296 (2020).
61. K. Gallagher, C. J. Hawkesworth, M. S. M. Mantovani, *J. Geophys. Res.*, in press.
62. Y. Gunnell, K. Gallagher, A. Carter, M. Widdowson, A. J. Hurford, Denudation history of the continental margin of western peninsular India since the early Mesozoic - reconciling apatite fission-track data with geomorphology. *Earth Planet. Sci. Lett.* **215**, 187–201 (2003).
63. BEICIP, Geological Map of Kenya (1987).
64. M. E. Moore, A. J. W. Gleadow, J. F. Lovering, Thermal evolution of rifted continental margins: new evidence from fission tracks in basement apatites from southeastern Australia. *Earth Planet. Sci. Lett.* **78**, 255–270 (1986).
65. P. A. van der Beek, J. Braun, K. Lambeck, Post-Palaeozoic uplift history of southeastern Australia revisited: Results from a process-based model of landscape evolution. *Aust. J. Earth Sci.* **46**, 157–172 (1999).
66. C. Persano, F. M. Stuart, P. Bishop, T. J. Dempster, Deciphering continental breakup in eastern Australia using low-temperature thermochronometers. *J. Geophys. Res. Solid Earth*. **110**, 1–17 (2005).
67. C. Persano, F. M. Stuart, P. Bishop, D. Barfod, Apatite (U-Th)/He age constraints on the development of the Great Escarpment on the southeastern Australian passive margin. *Earth Planet. Sci. Lett.* **200**, 79–90 (2002).
68. J. Braun, P. van der Beek, Evolution of passive margin escarpments: What can we learn from low-temperature thermochronology? *J. Geophys. Res.* **109**, 1–14 (2004).
69. M. Wildman, N. Cogné, R. Beucher, "Fission-Track Thermochronology Applied to the Evolution of Passive Continental Margins" in *Fission-Track Thermochronology and its Application to Geology* (Springer International Publishing, 2019; http://dx.doi.org/10.1007/978-3-319-89421-8_20), pp. 351–371.
70. P. Green, On the thermo-tectonic evolution of Northern England: evidence from fission track analysis. *Geol. Mag.* **123**, 493–506 (1986).
71. K. Gallagher, R. Brown, Denudation and uplift at passive margins: The record on the Atlantic Margin of southern Africa. *Philos. Trans. R. Soc. A Math. Phys. Eng. Sci.* **357**, 835–859 (1999).
72. P. F. Green, K. Lidmar-Bergström, P. Japsen, J. M. Bonow, J. A. Chalmers, Stratigraphic landscape analysis, thermochronology and the episodic development of elevated, passive continental margins. *Geol. Surv. Denmark Greenl. Bull.* **30**, 4–150 (2013).
73. P. F. Green, P. Japsen, J. A. Chalmers, J. M. Bonow, I. R. Duddy, Post-breakup burial and

exhumation of passive continental margins: Seven propositions to inform geodynamic models. *Gondwana Res.* **53**, 58–81 (2018).
74. M. McMillan, A. Gleadow, B. Kohn, C. Seiler, Post Gondwana breakup evolution of the SE Australia rifted margin revisited. *Terra Nov.* **32**, 109–121 (2020).
75. S. C. Boone, M. L. Balestrieri, B. Kohn, Tectono-Thermal Evolution of the Red Sea Rift. *Front. Earth Sci.* **9**, 1–9 (2021).
76. S. C. Boone, M. L. Balestrieri, B. Kohn, Thermo-tectonic imaging of the Gulf of Aden-Red Sea rift systems and Afro-Arabian hinterland. *Earth-Science Rev.* **222**, 103824 (2021).
77. W. Bosworth, "Geological Evolution of the Red Sea: Historical Background, Review, and Synthesis" in *The Red Sea* (2015), pp. 45–78.
78. D. F. Stockli, W. Bosworth, "Timing of extensional faulting along the magma-poor central and northern Red Sea rift margin—transition from regional extension to necking along a hyperextended rifted margin." in *Geological setting, palaeoenvironment and archaeology of the Red Sea* (Springer, 2018), pp. 81–111.
79. R. G. Bohannon, C. W. Naeser, D. L. Schmidt, R. A. Zimmermann, The timing of uplift, volcanism, and rifting peripheral to the Red Sea: A case for passive rifting? *J. Geophys. Res.* **94**, 1683–1701 (1989).
80. A. Daradich, J. X. Mitrovica, R. N. Pysklywec, S. D. Willett, A. M. Forte, Mantle flow, dynamic topography, and rift-flank uplift of Arabia. *Geology*. **31**, 901–904 (2003).
81. C. W. Naeser, The use of apatite and sphene for fission track age determinations. *Geol. Soc. Am. Bull.* **78**, 1523–1526 (1967).
82. N. Hasebe, J. Barbarand, K. Jarvis, A. Carter, A. J. Hurford, Apatite fission-track chronometry using laser ablation ICP-MS. *Chem. Geol.* **207**, 134–145 (2004).
83. D. M. Chew, R. a Donelick, Combined apatite fission track and U-Pb dating by LA-ICP-MS and its application in apatite provenance analysis. *Mineral. Assoc. Canada Short Course 42*, 219–247 (2012).
84. D. J. Gombosi, J. I. Garver, S. L. Baldwin, On the development of electron microprobe zircon fission-track geochronology. *Chem. Geol.* **363**, 312–321 (2014).
85. N. J. Evans, B. I. A. McInnes, B. McDonald, M. Danišík, T. Becker, P. Vermeesch, M. Shelley, E. Marillo-Sialer, D. B. Patterson, An in situ technique for (U-Th-Sm)/He and U-Pb double dating. *J. Anal. At. Spectrom.* **30**, 1636–1645 (2015).
86. M. Danišík, "Integration of Fission-Track Thermochronology with Other Geochronologic Methods on Single Crystals" in *Fission-Track Thermochronology and its Application to Geology* (Springer, 2019), pp. 93–108.

Supplementary Materials References

87. J. K. Hourigan, P. W. Reiners, M. T. Brandon, U-Th zonation-dependent alpha-ejection in (U-Th)/He chronometry. *Geochim. Cosmochim. Acta*. **69**, 3349–3365 (2005).
88. K. A. Farley, R. A. Wolf, L. T. Silver, The effects of long alpha-stopping distances on (U-Th)/He ages. *Geochim. Cosmochim. Acta*. **60**, 4223–4229 (1996).
89. J. Pickering, W. Matthews, E. Enkelmann, B. Guest, C. Sykes, B. M. Koblinger, Laser ablation (U-Th-Sm)/He dating of detrital apatite. *Chem. Geol.* **548**, 119683 (2020).
90. S. C. Boone, C. Seiler, B. P. Kohn, A. J. W. Gleadow, D. A. Foster, L. Chung, Influence of Rift Superposition on Lithospheric Response to East African Rift System Extension: Lapur Range, Turkana, Kenya. *Tectonics* (2018), doi:10.1002/2017TC004575.
91. S. C. Boone, B. P. Kohn, A. J. W. Gleadow, C. K. Morley, C. Seiler, D. A. Foster, L. Chung, Tectono-thermal evolution of a long-lived segment of the East African Rift System: Thermochronological insights from the North Lokichar Basin, Turkana, Kenya. *Tectonophysics*. **744**, 23–46 (2018).
92. S. C. Boone, B. P. Kohn, A. J. W. Gleadow, C. K. Morley, C. Seiler, D. A. Foster, Birth of

the East African Rift System: Nucleation of magmatism and strain in the Turkana Depression. *Geology*. **47** (2019), doi:10.1130/G46468.1.
93. D. A. Foster, A. J. W. Gleadow, The morphotectonic evolution of rift-margin mountains in central Kenya: Constraints from apatite fission-track thermochronology. *Earth Planet. Sci. Lett.* **113**, 157–171 (1992).
94. A. J. W. Gleadow, Fission track age of the KBS Tuff and associated hominid remains in northern Kenya. *Nature*. **284**, 225–230 (1980).
95. W. P. Noble, thesis, La Trobe University (1997).
96. D. A. Majer-Kielbaska, thesis, University of Melbourne (2015).
97. M. Wagner, R. Altherr, P. Van Den Haute, Apatite fission-track analysis of Kenyan basement rocks: constraints on the thermotectonic evolution of the Kenya dome. A reconnaissance study. *Tectonophysics*. **204**, 93–110 (1992).
98. E. Abbate, M. L. Balestrieri, G. Bigazzi, Morphostructural development of the Eritrean rift flank (southern Red Sea) inferred from apatite fission track analysis. *J. Geophys. Res.* **107**, 1–12 (2002).
99. B. P. Kohn, S. Feinstein, D. A. Foster, M. S. Steckler, M. Eyal, Thermal history of the eastern Gulf of Suez, II. Reconstruction from apatite fission track and 40Ar/39Ar K-feldspar measurements. *Tectonophysics*. **283**, 219–239 (1997).
100. B. Kohn, T. Weissbrod, L. Chung, K. Farley, S. Bodorkos, Low-temperature thermochronology of francolite: Insights into timing of Dead Sea Transform motion. *Terra Nov.* **31**, 205–219 (2019).
101. M. A. Menzies, J. Baker, D. Bosence, C. Dart, I. Davison, A. Hurford, M. Al'Kadasi, K. McClay, G. Nichols, A. Al'Subbary, A. Yelland, The timing of magmatism, uplift and crustal extension: Preliminary observations from Yemen. *Geol. Soc. Spec. Publ.* **68**, 293–304 (1992).
102. M. Menzies, K. Gallagher, A. Yelland, A. J. Hurford, Volcanic and nonvolcanic rifted margins of the Red Sea and Gulf of Aden: Crustal cooling and margin evolution in Yemen. *Geochim. Cosmochim. Acta*. **61**, 2511–2527 (1997).
103. N. Morag, I. Haviv, M. Eyal, B. P. Kohn, S. Feinstein, Early flank uplift along the Suez Rift: Implications for the role of mantle plumes and the onset of the Dead Sea Transform. *Earth Planet. Sci. Lett.* **516**, 56–65 (2019).
104. D. Naylor, M. Al-Rawi, G. Clayton, M. J. Fitzpatrick, P. F. Green, Hydrocarbon potential in Jordan. *J. Pet. Geol.* **36**, 205–236 (2013).
105. G. I. Omar, B. P. Kohn, T. M. Lutz, H. Faul, The cooling history of Silurian to Cretaceous alkaline ring complexes, south Eastern Desert, Egypt, as revealed by fission-track analysis. *Earth Planet. Sci. Lett.* **83**, 94–108 (1987).
106. G. I. Omar, M. S. Steckler, W. R. Buck, B. P. Kohn, Fission-track analysis of basement apatites at the western margin of the Gulf of Suez rift, Egypt: evidence for synchroneity of uplift and subsidence. *Earth Planet. Sci. Lett.* **94**, 316–328 (1989).
107. E. Szymanski, D. F. Stockli, P. R. Johnson, C. Hager, Thermochronometric evidence for diffuse extension and two-phase rifting within the Central Arabian Margin of the Red Sea Rift. *Tectonics*. **35**, 2863–2895 (2016).
108. P. Vermeesch, D. Avigad, M. O. McWilliams, 500 Myr of thermal history elucidated by multi-method detrital thermochronology of North Gondwana Cambrian sandstone (Eilat area, Israel). *Bull. Geol. Soc. Am.* **121**, 1204–1216 (2009).
109. E. Abbate, M. L. Balestrieri, G. Bigazzi, Uplifted rift-shoulder of the Gulf of Aden in northwestern Somalia: Palinspastic reconstructions supported by apatite fission-track data. *Mémoires du Muséum Natl. d'histoire Nat.* **186**, 629–640 (2001).
110. M. L. Balestrieri, F. M. Stuart, C. Persano, E. Abbate, G. Bigazzi, Geomorphic development of the escarpment of the Eritrean margin, southern Red Sea from combined

apatite fission-track and (U–Th)/He thermochronometry. *Earth Planet. Sci. Lett.* **231**, 97–110 (2005).
111. T. Abebe, M. L. Balestrieri, G. Bigazzi, The Central Main Ethiopian Rift is younger than 8 Ma: confirmation through apatite fission-track thermochronology. *Terra Nov.* **22**, 470–476 (2010).
112. M. L. Balestrieri, E. Abbate, G. Bigazzi, O. E. B. Ali, Thermochronological data from Sudan in the frame of the denudational history of the Nubian Red Sea margin. *Earth Surf. Process. Landforms*. **34**, 1279–1290 (2009).
113. A. V. Bojar, H. Fritz, S. Kargl, W. Unzog, Phanerozoic tectonothermal history of the Arabian-Nubian shield in the Eastern Desert of Egypt: Evidence from fission track and paleostress data. *J. African Earth Sci.* **34**, 191–202 (2002).
114. S. Feinstein, M. Eyal, B. P. Kohn, M. S. Steckler, K. M. Ibrahim, B. K. Moh'd, Y. Tian, Uplift and denudation history of the eastern Dead Sea rift fl ank , SW Jordan : Evidence from apatite fi ssion track thermochronometry. *Tectonics*. **32**, 1513–1528 (2013).
115. W. Ghebreab, A. Carter, A. J. Hurford, L. Jouniaux, Constraints for timing of extensional tectonics in the western margin of the Red Sea in Eritrea. *Earth Planet. Sci. Lett.* **200**, 107–119 (2002).
116. B. P. Kohn, M. Eyal, History of uplift of the crystalline basement of Sinai and its relation to opening of the Red Sea as revealed by fission track dating of apatites. *Earth Planet. Sci. Lett.* **52**, 129–141 (1981).

Supplementary Materials for

A global platform solution for Big Data in low-temperature thermochronology

Samuel C Boone[1,2], Fabian Kohlmann[3], Wayne Noble[3], Moritz Theile[3], Romain Beucher[4], Barry Kohn[1], Stijn Glorie[2], Martin Danišík[5], Renjie Zhou[6], Malcolm McMillan[1], Brent McInnes[5], Andrew Gleadow[1] and Angus Nixon[2]

[1]School of Geography, Earth and Atmospheric Sciences, The University of Melbourne, Melbourne, Victoria 3010, Australia.
[2]Department of Earth Sciences, University of Adelaide, Adelaide, SA 5005, Australia.
[3]Lithodat Pty Ltd, Melbourne, Victoria 3030, Australia.
[4]Australian National University, Research School of Earth Sciences, Canberra, Australia.
[5]John de Laeter Centre, Curtin University, Bentley, Western Australia 6102, Australia.
[6]University of Queensland, School of Earth and Environmental Sciences, Brisbane, Australia.

This PDF file includes:

Supplementary Text
Figure S1
Tables S1 to S8
References (29, 37, 39, 44, 48, 51, 63, 87-116)

Supplementary Text

Interpolation of Kenyan apatite fission-track mean track length data

Figure S1 shows an interpolation and the distribution of apatite fission-track mean track length data from Kenya, corresponding to the same area shown in Fig. 7b.

Relational data tables for fission-track and (U-Th)/He models

Presented below are the fission track (Tables S1-S5) and (U-Th)/He (Tables S6-S8) data tables for *AusGeochem*, including data type and unit specifications, and field descriptions. A diagram illustrating the relationships between these tables is presented in Fig. 1. The (U-Th)/He data model and corresponding tables (Tables S6-S8) were designed following the data reporting best-practices agreed on by the international expert community (*29*). While the fission-track model (Tables S1-S5) was designed after the recommended data reporting practices currently being prepared for submission to *Geological Society of America Bulletin* paper on “Reporting and Interpretation of Fission-Track Chronology Data”, led by B.K. and with co-authors S.B., M.D., and A.G. also being involved.

Data sources for regional compilations

Data sources for the regional thermochronology compilations shown in Figures 7 and 9 are listed in Tables S9 and S10, respectively.

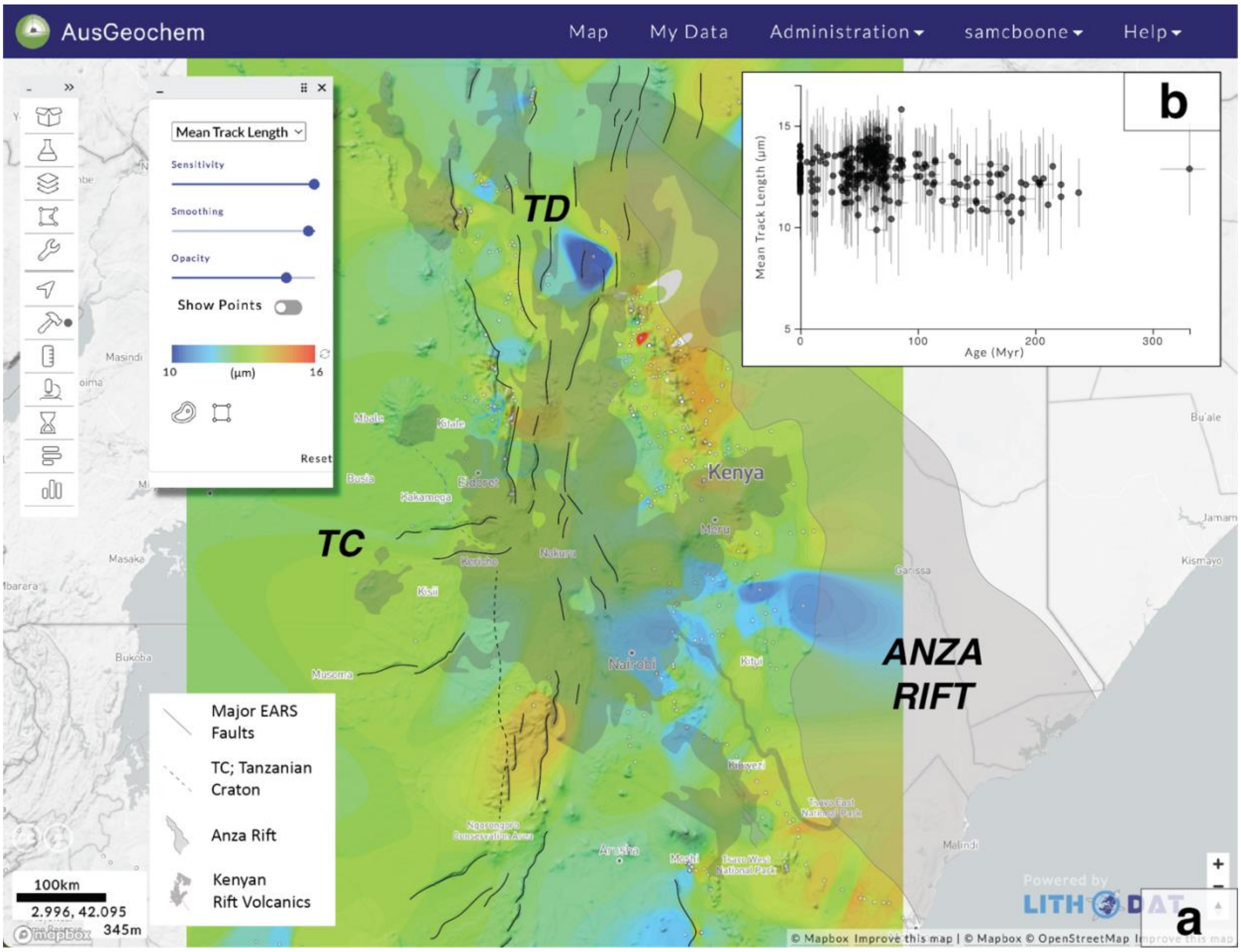

Figure S1. Interpolation (B) and distribution (C) of apatite fission-track mean track length data. Data sources are listed in the Table S9. All figure elements were exported from AusGeochem before being combined and annotated in a third-party graphics editor program. Distribution of Kenyan rift volcanic rocks from Beicip (*63*). TC = Tanzanian Craton; TD = Turkana Depression; EARS = East African Rift System.

Table S1.

(Meta-)data fields of the FT Data Point (Version 2.1.0), which record analytical metadata and fission track data on the rock sample scale. Blue fields are inherited from the *AusGeochem* Core Model (*44*).

Field	Datatype	Unit	Description
Sample ID	String		ID of sample analysed, usually assigned by sample collector
IGSN	String		International Geo Sample Number
Associated Literature	List		Database assigned ID for any particular publication
Laboratory	List		Lab name and/or Uni where analysis was conducted
Analyst	List		ORCID ID of analyst
Analysis Date-Time	Time		Date-time of analysis
Mineral Type	List		Mineral type analysed
Reference Material	List		Name of secondary reference material. NOTE: Only to be populated when datapoint refers to fission track analysis of a secondary reference material.
Batch ID (if applicable)	String		ID of analytical batch, allowing related unknown and secondary reference material results to be linked.
FT Characterisation Method	List		Method used to count and characterise fission tracks
FT Analytical Software	List		Software used to perform digital fission track analysis
FT Analytical Algorithm	List		The algorithm used to perform (semi-) automated FT counting
FT U Determination Technique	List		Analytical method used to measure uranium concentrations for FT age determinations
Etchant	List		Etchant chemical composition
Etchant Time	Float	seconds	Duration of etching
Etchant Temperature	Float	Celsius degrees	Temperature minerals were etched at
Cf Irradiation Y/N?	Boolean		Was the sample irradiated with ^{252}Cf?
No. of Grains	Integer		Total number of single grains analysed
Area	Float	cm^2	Total area of counting region
ρ_d	Float	cm^{-2}	Mean dosimeter track density
N_d	Integer		Total number of dosimeter tracks
ρ_s	Float	cm^{-2}	Mean spontaneous track density
N_s	Integer		Total number of spontaneous tracks
ρ_i	Float	cm^{-2}	Mean induced track density
N_i	Integer		Total number of induced tracks
Dosimeter	List		Dosimeter glass used for analysis (only relevant for EDM and population fission track methods)
Mean U Content	Float	ppm	Average U content of analysed grains
U Standard Deviation	Float	ppm	Standard deviation of average U content of analysed grains
Mean U/Ca Ratio	Float		Average U/Ca ratio of analysed grains
U/Ca Ratio Standard Deviation	Float		Standard deviation of average U/Ca ratio of analysed grains
Mean Dpar	Float	micrometres	Mean etch pit diameter parallel to crystallographic c-axis

Dpar Standard Error	Float	micrometres	Standard error of etch pit diameter parallel to crystallographic c-axis
Total Number of Dpar Measurements	Integer		The total number of Dpar measurements for the entire sample
Mean Dper	Float	micrometres	Mean etch pit diameter perpendicular to crystallographic c-axis
Dper Standard Error	Float	micrometres	Standard error of etch pit diameter perpendicular to crystallographic c-axis
Total Number of Dper Measurements	Integer		The total number of Dper measurements for the entire sample
Mean r_{mr0}	Float		Mean r_{mr0} of analysed grains, a parameter corresponding to annealing resistance of an apatite grain of certain composition (Carlson et al., 1999; Ketcham et al., 2007)
r_{mr0} Standard Deviation	Float		Standard deviation of r_{mr0}
r_{mr0} Equation	List		The equation used to determine the r_{mr0} and κ parameters
Mean κ	Float		Mean fitted parameter corresponding to annealing resistance of an apatite grain of certain composition (Carlson et al., 1999; Ketcham et al., 2007)
κ Standard Deviation	Float		Standard deviation of mean K parameter
FT Mean Age	Float	Ma	FT mean age
FT Mean Age Uncertainty	Float	Ma	FT mean age uncertainty
FT Central Age	Float	Ma	FT central age
FT Central Age Uncertainty	Float	Ma	FT central age uncertainty
FT Pooled Age	Float	Ma	FT pooled age
FT Pooled Age Uncertainty	Float	Ma	FT pooled age uncertainty
FT Population Age	Float	Ma	FT population age
FT Population Age Uncertainty	Float	Ma	FT population age uncertainty
Age Uncertainty Type	List		FT age uncertainty type
$P(\chi^2)$	Float	%	Chi-square test to statistically test the null-hypothesis that the analysed grains belong to one age population
Dispersion	Float		Measure of dispersion of single grain ages, ranging from 0 to 1
FT Age Equation	List		The equation used to determine FT age
ζ Calibration	Float	yr cm^2	Zeta for EDM or LA-ICP-MS zeta-calibrated fission track ages
ζ Calibration Uncertainty	Float	yr cm^2	Zeta uncertainty for EDM or LA-ICP-MS zeta-calibrated fission track ages
ζ Uncertainty Type	List		Zeta-calibration uncertainty type
R	Float	micrometres	R is the etchable fission track range used for determination of FT age via absolute dating approach
λ	List		Total ^{238}U decay constant used to determine FT age
λ_f	List		Fission decay constant used to determine FT age
q	Float		Detection efficiency factor
Irradiation Reactor	List		Name of irradiation reactor for EDM and population age determinations
Thermal Neutron Dose	Integer		Thermal neutron dose during sample irradiation (This parameter is only required for fission track ages determined using the Population Method)
MTL	Float	micrometres	**M**ean confined fission **T**rack **L**ength

No. Tracks	Integer		Number of tracks measured
MTL Standard Error	Float	micrometres	Standard error of mean confined track length
MTL Standard Deviation	Float	micrometres	Standard deviation of mean confined fission track length
Comment	Text		Additional information about analysis or data upload

Table S2.

FT Single Grain data table.

Field	Datatype	Unit	Description
Mount ID (FT Count)	String		Name or ID of sample mount used for fission track counting
Grain ID	String		Name or lab number of individual grain analysed
U Content	Float	ppm	Uranium content of analysed grain
U Uncertainty	Float	ppm	Uncertainty of uranium content of analysed grain
U/Ca Ratio	Float		U/Ca ratio of analysed grain
U/Ca Ratio Uncertainty	Float		Uncertainty of U/Ca ratio of analysed grain
U Uncertainty Type	List		Uncertainty type
FT Age	Float	Ma	FT age
FT Age Uncertainty	Float	Ma	FT age uncertainty
Age Uncertainty Type	List		Uncertainty type
r_{mr0}	Float		Parameter corresponding to annealing resistance of an apatite grain of certain composition (*37*, *39*)
κ	Float		Parameter corresponding to annealing resistance of an apatite grain of certain composition (*37*, *39*)
Comment	Text		Additional information about analysis or data upload

Table S3.

FT Count Data table. In addition to manual line-by-line and bulk uploading via the AusGeochem csv template, users can directly upload count data from *FastTracks* (*48*) using *FastTracks's* AusGeochemCount export data format.

Field	Datatype	Unit	Description
Grain ID	String		Name or lab number of individual grain analysed
Area	Float	cm^2	Total area of counting region
ρ_s	Float	cm^{-2}	Spontaneous track density
N_s	Integer		Number of spontaneous tracks
ρ_i	Float	cm^{-2}	Induced track density
N_i	Integer		Number of induced tracks
Dpar	Float	micrometres	Modal etch pit diameter parallel to crystallographic c-axis
Dpar Uncertainty	Float	micrometres	Uncertainty of etch pit diameter parallel to crystallographic c-axis
Number of Dpar Measurements	Integer		Number of Dpar measurements
Dper	Float	micrometres	Modal etch pit diameter perpendicular to crystallographic c-axis
Dper Uncertainty	Float	micrometres	Uncertainty of etch pit diameter perpendicular to crystallographic c-axis
Number of Dper Measurements	Integer		Number of Dper measurements
Uncertainty Type	List		Dpar and Dper measurement uncertainty type
Comment	Text		Additional information about analysis or data upload

Table S4.
FT Length Data table. In addition to manual line-by-line and bulk uploading via the AusGeochem csv template, users can directly upload length data from *FastTracks* (*48*) using FastTracks's AusGeochemLength export data format.

Field	Datatype	Unit	Description
Mount ID (FT Lengths)	String		Name or ID of sample mount used for fission track length measurements
Etchant Time	Float	seconds	Duration of etching
Grain ID	String		Name or lab number of individual grain analysed
Track ID	String		The name or lab number of the measured track
Track Type	List		Type of track measurement (e.g., semi-track, confined track-in-track, confined track-in-cleavage)
Apparent Length	Float	micrometres	Apparent length measured parallel to grain surface
Corrected z-Depth	Float	micrometres	Distance in z-direction between track end points, corrected for refractive index of analysed mineral
Track Length	Float	micrometres	Fission track length
Azimuth	Float	degrees	Azimuth of track
Dip	Float	degrees	Dip of track
c-Axis Angle	Float	degrees	Angle of fission track to crystallographic c-axis
c-Axis Angle Corrected Length	Float	micrometres	c-axis corrected fission track length
Dpar	Float	micrometres	Modal etch pit diameter parallel to crystallographic c-axis
Dpar Uncertainty	Float	micrometres	Uncertainty of etch pit diameter parallel to crystallographic c-axis
Number of Dpar Measurements	Integer		The number of Dpar measurements
Dper	Float	micrometres	Modal etch pit diameter perpendicular to crystallographic c-axis
Dper Uncertainty	Float	micrometres	Uncertainty of etch pit diameter perpendicular to crystallographic c-axis
Number of Dper Measurements	Integer		The number of Dper measurements
Uncertainty Type	List		Dpar and Dper measurement uncertainty type
r_{mr0}	Float		Parameter corresponding to annealing resistance of an apatite grain of certain composition (*37*, *39*)
κ	Float		Fitted parameter corresponding to annealing resistance of an apatite grain of certain composition (*37*, *39*)
Comment	Text		Additional information about analysis or data upload

Table S5.
FT Binned Length Data table, which is designed to accommodate the uploading of legacy data in cases where only confined track length histograms were provided in either one or two micron bins.

Field	Datatype	Unit	Description
Mount ID (FT Lengths)	String		Name or ID of sample mount used for fission track length measurements
Etchant Time	Float	seconds	Duration of etching
Dpar	Float	micrometres	Modal etch pit diameter parallel to crystallographic c-axis
Dpar Uncertainty	Float	micrometres	Uncertainty of etch pit diameter parallel to crystallographic c-axis
Number of Dpar Measurements	Integer		The number of Dpar measurements
Dper	Float	micrometres	Modal etch pit diameter perpendicular to crystallographic c-axis
Dper Uncertainty	Float	micrometres	Uncertainty of etch pit diameter perpendicular to crystallographic c-axis
Number of Dper Measurements	Integer		The number of Dper measurements
Uncertainty Type	List		Dpar and Dper measurement uncertainty type
0-1 μm Bin	Integer		Number of measured confined tracks in 0 to 1 micron bin
1-2 μm Bin	Integer		Number of measured confined tracks in 1 to 2 micron bin
2-3 μm Bin	Integer		Number of measured confined tracks in 2 to 3 micron bin
3-4 μm Bin	Integer		Number of measured confined tracks in 3 to 4 micron bin
4-5 μm Bin	Integer		Number of measured confined tracks in 4 to 5 micron bin
5-6 μm Bin	Integer		Number of measured confined tracks in 5 to 6 micron bin
6-7 μm Bin	Integer		Number of measured confined tracks in 6 to 7 micron bin
7-8 μm Bin	Integer		Number of measured confined tracks in 7 to 8 micron bin
8-9 μm Bin	Integer		Number of measured confined tracks in 8 to 9 micron bin
9-10 μm Bin	Integer		Number of measured confined tracks in 9 to 10 micron bin
10-11 μm Bin	Integer		Number of measured confined tracks in 10 to 11 micron bin
11-12 μm Bin	Integer		Number of measured confined tracks in 11 to 12 micron bin
12-13 μm Bin	Integer		Number of measured confined tracks in 12 to 13 micron bin
13-14 μm Bin	Integer		Number of measured confined tracks in 13 to 14 micron bin
14-15 μm Bin	Integer		Number of measured confined tracks in 14 to 15 micron bin
15-16 μm Bin	Integer		Number of measured confined tracks in 15 to 16 micron bin
16-17 μm Bin	Integer		Number of measured confined tracks in 16 to 17 micron bin
17-18 μm Bin	Integer		Number of measured confined tracks in 17 to 18 micron bin

18-19 µm Bin	Integer		Number of measured confined tracks in 18 to 19 micron bin
19-20 µm Bin	Integer		Number of measured confined tracks in 19 to 29 micron bin
Comment	Text		Additional information about analysis or data upload

Table S6.
(Meta-)data fields of the He Data Point, which record analytical metadata and (U-Th)/He data on the rock sample scale. Blue fields are inherited from the *AusGeochem* Core Model (*44*).

Field	Datatype	Unit	Description
Sample ID	String		ID of sample analysed, usually assigned by sample collector
IGSN	String		International Geo Sample Number
Associated Literature	List		Database assigned ID for any particular publication
Laboratory	List		Lab name and/or Uni where analysis was conducted
Analyst	List		ORCID ID of analyst
Analysis Date-Time	Time		Date-time of analysis
Mineral Type	List		Mineral type analysed
Mount ID (if appropriate)	String		Name or ID of sample mount used for in-situ (U-Th)/He analysis
Reference Material	List		Name of secondary reference material. NOTE: Only to be populated when datapoint refers to (U-Th)/He analysis of a secondary reference material.
Batch ID (if applicable)	String		ID of analytical batch, allowing related unknown and secondary reference material results to be linked.
Number of Aliquots	Integer		Number of aliquots analysed
Mean Uncorrected He Age	Float	Ma	Mean uncorrected He age
Mean Uncorrected He Age Uncertainty	Float	Ma	Uncertainty of mean uncorrected He age
Mean Uncorrected Age Uncertainty Type	List		Mean Uncorrected Age Uncertainty Type
Weighted Uncorrected Mean He Age	Float	Ma	Weighted mean uncorrected He age
Weighted Uncorrected Mean He Age Uncertainty	Float	Ma	Uncertainty of weighted mean uncorrected He age
Weighted Uncorrected Mean Age Uncertainty Type	List		Weighted Uncorrected Mean Age Uncertainty Type
MSWD of Weighted Mean Uncorrected Age	Float		Mean Square Weighted Deviation for reported weighted mean uncorrected He age
Weighted Mean Uncorrected Age 95% Confidence Interval	Float	Ma	The 95% confidence interval of the weighted mean uncorrected age
Weighted Mean Uncorrected Age P(χ^2)	Float	Percentage	Chi-squared test to statistically test the null-hypothesis that the analysed aliquots belong to one age population
Uncorrected Age Interquartile Range (IQR)	Float	Ma	Interquartile range (IQR) of aliquot He ages, a robust measure of statistical dispersion in intrasample He datasets (*51*).
Mean Corrected He Age	Float	Ma	Mean corrected He age
Mean Corrected He Age Uncertainty	Float	Ma	Uncertainty of mean corrected He age
Uncertainty Type	List		Uncertainty type
Weighted Mean Corrected He Age	Float	Ma	Weighted mean corrected He age
Weighted Mean Corrected He Age Uncertainty	Float	Ma	Uncertainty of weighted mean corrected He age

Uncertainty Type	List		Uncertainty type
MSWD of Weighted Mean Corrected Age	Float		Mean Square Weighted Deviation for reported weighted mean corrected He age
Weighted Mean Corrected Age 95% Confidence Interval	Float	Ma	The 95% confidence interval of the weighted mean corrected age
Weighted Mean Corrected Age P(χ^2)	Float	Percentage	Chi-square test to statistically test the null-hypothesis that the analysed aliquots belong to one age population
Corrected Age Interquartile Range (IQR)	Float	Ma	Interquartile range (IQR) of aliquot He ages, a robust measure of statistical dispersion in intrasample He datasets (*51*).
Uncertainty Factors Comment	String		Describe the factors included in uncertainty calculations (e.g., propagated precision on repeat measurements of the sample, blanks, spikes, and reference materials). See Section 7 in Flowers et al. (*29*) for guidance.
Ablation Pit Measuring Technique	List		The method used to measure ablation pit volumes. Only applicable for in-situ (U-Th)/He analysis.
Pit Volume Determination Software	List		The software used to calculate ablation pit volumes. Only applicable for in-situ (U-Th)/He analysis.
In-Situ He Measurement Technique	List		The method used to measure 4He content in-situ. Only applicable for in-situ (U-Th)/He analysis.
In-Situ Parent Isotope Measurement Technique	List		The method used to measure parent isotope content in-situ. Only applicable for in-situ (U-Th)/He analysis.
Grain Dimensions Equations Reference	List		Reference to equations used for calculating surface area and volume of grains
Alpha Stopping Distances Reference	List		Reference to alpha stopping distances used in calculations
FT Equation	List		Alpha-ejection correction (FT) equation used
Rsv Equation	List		Equation used to calculate an equivalent spherical radius using the equivalent surface area to volume ratio approach
Rft Equation	List		Equation used to calculate an equivalent spherical radius using the radius of a sphere with an equivalent FT correction
eU Equation	List		Equation used to calculate eU concentration
He Age Equation	List		Approach employed to calculate the reported He age
Corrected He Age Determination Method	List		The method used to calculate the corrected He age
Comment	Text		Additional information about analysis or data upload

Table S7.
He Whole Grain data table.

Field	Datatype	Unit	Description
Aliquot ID	String		Name or lab number of analysed aliquot (if available)
Aliquot Type	List		The type of aliquot analysed, i.e., single-grain, multi-grain or unknown
Number of Aliquot Grains	Integer		Number of grains in aliquot (only relevant for multi-grain aliquots)
Crystal Fragmentation	List		Is the crystal whole, fragmented, abraded, mixed (in the case of multi-grain aliquots) or unknown?
Aliquot Morphology	List		Morphology of analysed aliquot grain(s)
Assumed Aliquot Geometry	List		Assumed geometry of grain(s)
Aliquot Length	Float	µm	Length of analysed grain(s) (average value for multi-grain aliquots)
Average Aliquot Length Standard Deviation	Float	µm	One standard deviation of average length of analysed grains (only relevant for multi-grain aliquots)
Aliquot Width	Float	µm	Width of analysed grain(s) (average value for multi-grain aliquots)
Average Aliquot Width Standard Deviation	Float	µm	One standard deviation of average width of analysed grains (only relevant for multi-grain aliquots)
Aliquot Height	Float	µm	Height (second width) of analysed grain(s), if measured (average value for multi-grain aliquots)
Average Aliquot Height Standard Deviation	Float	µm	One standard deviation of average height (second width) of analysed grains, if measured (only relevant for multi-grain aliquots)
Surface Area	Float	μm^2	Surface area of analysed grain(s) (average value for multi-grain aliquots)
Average Surface Area Standard Deviation	Float	μm^2	One standard deviation of average surface area of analysed grains (only relevant for multi-grain aliquots)
Volume	Float	μm^3	Estimated volume of analysed grain(s) (average value for multi-grain aliquots)
Average Volume Standard Deviation	Float	μm^3	One standard deviation of average estimated volume of analysed grains (only relevant for multi-grain aliquots)
Pyramidal Termination Height 1	Float	µm	Pyramidal termination 1 height of analysed grain(s), if measured (average value for multi-grain aliquots)
Average Pyramidal Termination Height 1 Standard Deviation	Float	µm	One standard deviation of average pyramidal termination 1 height of analysed grains, if measured (only relevant for multi-grain aliquots)
Pyramidal Termination Height 2	Float	µm	Pyramidal termination 2 height of analysed grain(s), if measured (average value for multi-grain aliquots)
Average Pyramidal Termination Height 2 Standard Deviation	Float	µm	One standard deviation of average pyramidal termination 2 height of analysed grains, if measured (only relevant for multi-grain aliquots)
V/S Ratio	Float		Volume to surface area ratio of analysed grain(s); see eq. 15 in Hourigan et al. (87)
F_T	Float		Mass-weighted mean alpha ejection correction (FT) of aliquot (88)
F_T Uncertainty	Float		Estimated Uncertainty of alpha ejection correction. E.g., Farley et al. (88) recommended an estimated

			FT error of 5% for FT > 0.6, 10% for FT < 0.6, 15% for FT < 0.5
Uncertainty Type	List		Uncertainty type
R_{SV}	Float	µm	Average equivalent spherical radius of analysed aliquot, computed as the radius of a sphere with an equivalent surface area to volume ratio as analysed aliquot
R_{FT}	Float	µm	Average equivalent spherical radius of analysed aliquot, computed as the radius of a sphere with an equivalent FT correction
Assumed Mineral Density	Float	g/cm^3	Assumed mineral density used to determine mass using the dimensional approach
Ca Content	Float	ng	Total Ca content of aliquot in nanograms, if measured. Usually only measured if aliquot mass is determined stoichiometrically.
Ca Content Uncertainty	Float	ng	Total Ca content uncertainty, if measured. Usually only measured if aliquot mass is determined stoichiometrically.
Uncertainty Type	List		Uncertainty type
Zr Content	Float	ng	Total Zr content of aliquot in nanograms, if measured. Usually only measured if aliquot mass is determined stoichiometrically.
Zr Content Uncertainty	Float	ng	Total Zr content uncertainty, if measured. Usually only measured if aliquot mass is determined stoichiometrically.
Uncertainty Type	List		Uncertainty type
Assumed Mineral Chemical Formula	Float		Assumed chemical formula for mineral used to determine mass using the stoichiometric approach (e.g., for apatite, $Ca_5(PO_4)_3(OH)$ or $Ca_5(PO_4)_3F$ or $Ca_5(PO_4)_3Cl$.
Estimated Aliquot Mass	Float	mg	Estimated aliquot mass
Estimated Aliquot Mass Uncertainty	Float	mg	Uncertainty of estimated aliquot mass
Uncertainty Type	List		Uncertainty type
^{4}He Absolute Amount	Float	ncc	Absolute He content of aliquot
^{4}He Absolute Amount Uncertainty	Float	ncc	Uncertainty of absolute He content of aliquot
Uncertainty Type	List		Uncertainty type
^{4}He Concentration	Float	nmol/g	^{4}He concentration of aliquot
^{4}He Concentration Uncertainty	Float	nmol/g	^{4}He concentration uncertainty of aliquot
Uncertainty Type	List		Uncertainty type
U Absolute Amount	Float	ng	Absolute amount of Uranium (^{238}U + ^{235}U) in aliquot
U Absolute Amount Uncertainty	Float	ng	Uncertainty of absolute amount of Uranium (^{238}U + ^{235}U) in aliquot
Uncertainty Type	List		Uncertainty type
U Concentration	Float	ppm	Uranium (^{238}U + ^{235}U) concentration of aliquot, calculated as µg/g
U Concentration Uncertainty	Float	ppm	Uncertainty of Uranium (^{238}U + ^{235}U) concentration of aliquot, calculated as µg/g
Uncertainty Type	List		Uncertainty type
Th Absolute Amount	Float	ng	Absolute amount of Thorium (^{232}Th) in aliquot
Th Absolute Amount Uncertainty	Float	ng	Uncertainty of absolute amount of Thorium (^{232}Th) in aliquot
Uncertainty Type	List		Uncertainty type
Th Concentration [ppm]	Float	ppm	Thorium (^{232}Th) concentration of aliquot, calculated as µg/g

Th Concentration Uncertainty [ppm]	Float	ppm	Uncertainty of Thorium (^{232}Th) concentration of aliquot, calculated as µg/g
Uncertainty Type	List		Uncertainty type
Sm Absolute Amount	Float	ng	Absolute amount of Sumerium (^{147}Sm) in aliquot
Sm Absolute Amount Uncertainty	Float	ng	Uncertainty of absolute amount of Sumerium (^{147}Sm) in aliquot
Uncertainty Type	List		Uncertainty type
Sm Concentration	Float	ppm	Sumerium (^{147}Sm) concentration of aliquot, calculated as µg/g
Sm Concentration Uncertainty	Float	ppm	Uncertainty of Sumerium (^{147}Sm) concentration of aliquot, calculated as µg/g
Uncertainty Type	List		Uncertainty type
Th/U	Float		Thorium/Uranium ratio
eU	Float	ppm	Effective uranium concentration
eU Uncertainty	Float	ppm	Effective uranium concentration uncertainty
Uncertainty Type	List		Uncertainty type
Uncorrected He Age	Float	Ma	Uncorrected He age
Uncorrected He Age Uncertainty	Float	Ma	Total analytical uncertainty on uncorrected He age (before FT correction). This should include the propagated uncertainties on the absolute amounts of daughter and parent. See Section 7 in Flowers et al. (*29*) for guidance.
Uncertainty Type	List		Uncertainty type
Corrected He Age	Float	Ma	FT corrected He age
Total Analytical Uncertainty (Corrected Age)	Float	Ma	Total analytical uncertainty on corrected He age (FT corrected). This should include the propagated uncertainties on the absolute amounts of daughter and parent. See Section 7 in Flowers et al. (*29*) for guidance.
Uncertainty Type	List		Uncertainty type
Total Analytical Uncertainty + FT (Corrected Age)	Float	Ma	Total analytical uncertainty on corrected He age (FT corrected) including an estimated uncertainty for Ft correction. This should include the propagated uncertainties on the absolute amounts of daughter and parent. See Section 7 in Flowers et al. (*29*) for guidance.
Uncertainty Type	List		Uncertainty type
Comment	Text		Additional information about analysis or data upload

Table S8.
He In-Situ data table.

Field	Datatype	Unit	Description
Grain ID	String		Name or lab number of analysed grain (if available)
Pit ID	String		Identifier for analysed pit
Crystal Fragmentation	List		Is the crystal whole, fragmented, abraded, or unknown?
He Measurement Pit Volume	Float	μm^3	Volume of ablation pit for He content measurement
He Measurement Pit Volume Uncertainty	Float	μm^3	Uncertainty of ablation pit volume for He content measurement
Uncertainty Type	List		Uncertainty type
Parent Isotopes Measurement Pit Volume	Float	μm^3	Volume of ablation pit for parent isotopic content measurement (if measured)
Parent Isotopes Measurement Pit Volume Uncertainty	Float	μm^3	Uncertainty of ablation pit volume for parent isotopic content measurement (if measured)
Uncertainty Type	List		Uncertainty type
^{4}He Absolute Amount	Float	ncc	Absolute He content
^{4}He Absolute Amount Uncertainty	Float	ncc	Uncertainty of absolute He content
Uncertainty Type	List		Uncertainty type
^{4}He Concentration	Float	nmol/g	^{4}He concentration
^{4}He Concentration Uncertainty	Float	nmol/g	^{4}He concentration uncertainty
Uncertainty Type	List		Uncertainty type
U Absolute Amount	Float	ng	Absolute amount of Uranium (^{238}U + ^{235}U)
U Absolute Amount Uncertainty	Float	ng	Uncertainty of absolute amount of Uranium (^{238}U + ^{235}U)
Uncertainty Type	List		Uncertainty type
U Concentration	Float	ppm	Uranium (^{238}U + ^{235}U) concentration, calculated as µg/g
U Concentration Uncertainty	Float	ppm	Uncertainty of Uranium (^{238}U + ^{235}U) concentration, calculated as µg/g
Uncertainty Type	List		Uncertainty type
Th Absolute Amount	Float	ng	Absolute amount of Thorium (^{232}Th)
Th Absolute Amount Uncertainty	Float	ng	Uncertainty of absolute amount of Thorium (^{232}Th)
Uncertainty Type	List		Uncertainty type
Th Concentration [ppm]	Float	ppm	Thorium (^{232}Th) concentration, calculated as µg/g
Th Concentration Uncertainty [ppm]	Float	ppm	Uncertainty of Thorium (^{232}Th) concentration, calculated as µg/g
Uncertainty Type	List		Uncertainty type
Sm Absolute Amount	Float	ng	Absolute amount of Sumerium (^{147}Sm)
Sm Absolute Amount Uncertainty	Float	ng	Uncertainty of absolute amount of Sumerium (^{147}Sm)
Uncertainty Type	List		Uncertainty type
Sm Concentration	Float	ppm	Sumerium (^{147}Sm) concentration, calculated as µg/g
Sm Concentration Uncertainty	Float	ppm	Uncertainty of Sumerium (^{147}Sm) concentration, calculated as µg/g
Uncertainty Type	List		Uncertainty type
eU	Float	ppm	Effective uranium concentration
eU Uncertainty	Float	ppm	Effective uranium concentration uncertainty
Uncertainty Type	List		Uncertainty type

Relationship of He and Parent Isotopes Measurement Locations	List		The spatial relationship between the He and parent isotope measurement beam locations/ablation pits
Uncorrected He Age	Float	Ma	Uncorrected He age
Uncorrected He Age Uncertainty	Float	Ma	Total analytical uncertainty on uncorrected He age (before FT correction). This should include the propagated uncertainties on the absolute amounts of daughter and parent. See Section 7 in Flowers et al. (2022) for guidance.
Uncertainty Type	List		Uncertainty type
Age Calibration Factor (if applicable)	Float		He Age Calibration factor, if applicable (following the methods of Pickering et al. (*89*)
Calibration Factor Corrected He Age (if applicable)	Float	Ma	Calibration factor corrected He age (if calculated)
Calibration Factor Corrected He Age Uncertainty (if applicable)	Float	Ma	Total analytical uncertainty on corrected He age (FT corrected). This should include the propagated uncertainties on the absolute amounts of daughter and parent. See Section 7 in Flowers et al. (2022) for guidance.
Uncertainty Type	List		Uncertainty type
Comment	Text		Additional information about analysis or data upload

Table S9.

Apatite fission-track data sources for Kenyan compilation.

S. C. Boone, C. Seiler, B. P. Kohn, A. J. W. Gleadow, D. A. Foster, L. Chung, Influence of Rift Superposition on Lithospheric Response to East African Rift System Extension: Lapur Range, Turkana, Kenya. *Tectonics* (2018), doi:10.1002/2017TC004575.
S. C. Boone, B. P. Kohn, A. J. W. Gleadow, C. K. Morley, C. Seiler, D. A. Foster, L. Chung, Tectono-thermal evolution of a long-lived segment of the East African Rift System: Thermochronological insights from the North Lokichar Basin, Turkana, Kenya. *Tectonophysics*. **744**, 23–46 (2018).
S. C. Boone, B. P. Kohn, A. J. W. Gleadow, C. K. Morley, C. Seiler, D. A. Foster, Birth of the East African Rift System: Nucleation of magmatism and strain in the Turkana Depression. *Geology*. **47** (2019), doi:10.1130/G46468.1.
D. A. Foster, A. J. W. Gleadow, The morphotectonic evolution of rift-margin mountains in central Kenya: Constraints from apatite fission-track thermochronology. *Earth Planet. Sci. Lett.* **113**, 157–171 (1992).
D. A. Foster, J. W. Gleadow, Structural framework and denudation history of the flanks of the Kenya and Anza Rifts, East Africa. *Tectonics*. **15**, 258–271 (1996).
A. J. W. Gleadow, Fission track age of the KBS Tuff and associated hominid remains in northern Kenya. *Nature*. **284**, 225–230 (1980).
W. P. Noble, Post Pan African Tectonic Evolution of Eastern Africa: An Apatite Fission Track Study. PhD Thesis, La Trobe University (1997).
D. A. Majer-Kielbaska, Low temperature thermochronology of the northernmost Mozambique Belt, Kenya. MSc thesis, University of Melbourne (2015)
V. Torres Acosta, A. Bande, E. R. Sobel, M. Parra, T. F. Schildgen, F. Stuart, M. R. Strecker, Cenozoic extension in the Kenya Rift from low-temperature thermochronology: Links to diachronous spatiotemporal evolution of rifting in East Africa. *Tectonics*. **34**, 2367–2386 (2015).
M. Wagner, R. Altherr, P. Van Den Haute, Apatite fission-track analysis of Kenyan basement rocks: constraints on the thermotectonic evolution of the Kenya dome. A reconnaissance study. *Tectonophysics*. **204**, 93–110 (1992).

Table S10.

Fission-track and (U-Th)/He data sources for Red Sea compilation.

R. G. Bohannon, C. W. Naeser, D. L. Schmidt, R. A. Zimmermann, The timing of uplift, volcanism, and rifting peripheral to the Red Sea: A case for passive rifting? *J. Geophys. Res.* **94**, 1683–1701 (1989).
E. Abbate, M. L. Balestrieri, G. Bigazzi, Morphostructural development of the Eritrean rift flank (southern Red Sea) inferred from apatite fission track analysis. *J. Geophys. Res.* **107**, 1–12 (2002).
E. Abbate, M. L. Balestrieri, G. Bigazzi, Uplifted rift-shoulder of the Gulf of Aden in northwestern Somalia: Palinspastic reconstructions supported by apatite fission-track data. *Mémoires du Muséum Natl. d'histoire Nat.* **186**, 629–640 (2001).
M. L. Balestrieri, F. M. Stuart, C. Persano, E. Abbate, G. Bigazzi, Geomorphic development of the escarpment of the Eritrean margin, southern Red Sea from combined apatite fission-track and (U–Th)/He thermochronometry. *Earth Planet. Sci. Lett.* **231**, 97–110 (2005).
T. Abebe, M. L. Balestrieri, G. Bigazzi, The Central Main Ethiopian Rift is younger than 8 Ma: confirmation through apatite fission-track thermochronology. *Terra Nov.* **22**, 470–476 (2010).
M. L. Balestrieri, E. Abbate, G. Bigazzi, O. E. B. Ali, Thermochronological data from Sudan in the frame of the denudational history of the Nubian Red Sea margin. *Earth Surf. Process. Landforms*. **34**, 1279–1290 (2009).
A. V. Bojar, H. Fritz, S. Kargl, W. Unzog, Phanerozoic tectonothermal history of the Arabian-Nubian shield in the Eastern Desert of Egypt: Evidence from fission track and paleostress data. *J. African Earth Sci.* **34**, 191–202 (2002).
S. Feinstein, M. Eyal, B. P. Kohn, M. S. Steckler, K. M. Ibrahim, B. K. Moh'd, Y. Tian, Uplift and denudation history of the eastern Dead Sea rift fl ank , SW Jordan : Evidence from apatite fi ssion track thermochronometry. *Tectonics*. **32**, 1513–1528 (2013).
W. Ghebreab, A. Carter, A. J. Hurford, L. Jouniaux, Constraints for timing of extensional tectonics in the western margin of the Red Sea in Eritrea. *Earth Planet. Sci. Lett.* **200**, 107–119 (2002).
B. P. Kohn, M. Eyal, History of uplift of the crystalline basement of Sinai and its relation to opening of the Red Sea as revealed by fission track dating of apatites. *Earth Planet. Sci. Lett.* **52**, 129–141 (1981).
B. P. Kohn, S. Feinstein, D. A. Foster, M. S. Steckler, M. Eyal, Thermal history of the eastern Gulf of Suez, II. Reconstruction from apatite fission track and 40Ar/39Ar K-feldspar measurements. *Tectonophysics*. **283**, 219–239 (1997).
B. Kohn, T. Weissbrod, L. Chung, K. Farley, S. Bodorkos, Low-temperature thermochronology of francolite: Insights into timing of Dead Sea Transform motion. *Terra Nov.* **31**, 205–219 (2019).
M. A. Menzies, J. Baker, D. Bosence, C. Dart, I. Davison, A. Hurford, M. Al'Kadasi, K. McClay, G. Nichols, A. Al'Subbary, A. Yelland, The timing of magmatism, uplift and crustal extension: Preliminary observations from Yemen. *Geol. Soc. Spec. Publ.* **68**, 293–304 (1992).
M. Menzies, K. Gallagher, A. Yelland, A. J. Hurford, Volcanic and nonvolcanic rifted margins of the Red Sea and Gulf of Aden: Crustal cooling and margin evolution in Yemen. *Geochim. Cosmochim. Acta*. **61**, 2511–2527 (1997).
N. Morag, I. Haviv, M. Eyal, B. P. Kohn, S. Feinstein, Early flank uplift along the Suez Rift: Implications for the role of mantle plumes and the onset of the Dead Sea Transform. *Earth Planet. Sci. Lett.* **516**, 56–65 (2019).
D. Naylor, M. Al-Rawi, G. Clayton, M. J. Fitzpatrick, P. F. Green, Hydrocarbon potential in Jordan. *J. Pet. Geol.* **36**, 205–236 (2013).
G. I. Omar, B. P. Kohn, T. M. Lutz, H. Faul, The cooling history of Silurian to Cretaceous alkaline ring complexes, south Eastern Desert, Egypt, as revealed by fission-track analysis. *Earth Planet. Sci. Lett.* **83**, 94–108 (1987).
G. I. Omar, M. S. Steckler, W. R. Buck, B. P. Kohn, Fission-track analysis of basement apatites at the western margin of the Gulf of Suez rift, Egypt: evidence for synchroneity of uplift and subsidence. *Earth Planet. Sci. Lett.* **94**, 316–328 (1989).
E. Szymanski, D. F. Stockli, P. R. Johnson, C. Hager, Thermochronometric evidence for diffuse extension and two-phase rifting within the Central Arabian Margin of the Red Sea Rift. *Tectonics*. **35**, 2863–2895 (2016).
P. Vermeesch, D. Avigad, M. O. McWilliams, 500 Myr of thermal history elucidated by multi-method detrital thermochronology of North Gondwana Cambrian sandstone (Eilat area, Israel). *Bull. Geol. Soc. Am.* **121**, 1204–1216 (2009).

References

29. R. M. Flowers, P. K. Zeitler, M. Danišík, P. W. Reiners, C. Gautheron, R. A. Ketcham, J. R. Metcalf, D. F. Stockli, E. Enkelmann, R. W. Brown, (U-Th)/He chronology: Part 1. Data, uncertainty, and reporting. *GSA Bull.*, 1–33 (2022).
37. W. D. Carlson, R. A. Donelick, R. A. Ketcham, Variability of apatite fission-track annealing kinetics: II. Crystallographic orientation effects. *Am. Mineral.* **84**, 1224–1234 (1999).
39. R. A. Ketcham, A. Carter, R. A. Donelick, J. Barbarand, A. J. Hurford, Improved modeling of fission-track annealing in apatite. *Am. Mineral.* **92**, 799–810 (2007).
44. S. C. Boone, H. Dalton, A. Prent, F. Kohlmann, M. Theile, Y. Gréau, G. Florin, W. Noble, S. Hodgekiss, B. Ware, D. Phillips, B. Kohn, S. O'Reilly, A. Gleadow, B. McInnes, T. Rawling, AusGeochem: An Open Platform for Geochemical Data Preservation, Dissemination and Synthesis. *Geostand. Geoanalytical Res.* (2022), doi:10.1111/ggr.12419.
48. A. J. W. Gleadow, S. J. Gleadow, D. X. Belton, B. P. Kohn, M. S. Krochmal, R. W. Brown, Coincidence mapping – a key strategy for the automatic counting of fission tracks in natural minerals. *Geol. Soc. London Spec. Publ. Thermochronological Methods From Palaeotemperature Constraints to Landsc. Evol. Model.* **324**, 25–36 (2009).
51. S. C. Boone, M. L. Balestrieri, B. P. Kohn, G. Corti, A. J. W. Gleadow, C. Seiler, Tectonothermal Evolution of the Broadly Rifted Zone, Ethiopian Rift. *Tectonics*. **38**, 1070–1100 (2019).
63. BEICIP, Geological Map of Kenya (1987).
87. J. K. Hourigan, P. W. Reiners, M. T. Brandon, U-Th zonation-dependent alpha-ejection in (U-Th)/He chronometry. *Geochim. Cosmochim. Acta*. **69**, 3349–3365 (2005).
88. K. A. Farley, R. A. Wolf, L. T. Silver, The effects of long alpha-stopping distances on (U-Th)/He ages. *Geochim. Cosmochim. Acta*. **60**, 4223–4229 (1996).
89. J. Pickering, W. Matthews, E. Enkelmann, B. Guest, C. Sykes, B. M. Koblinger, Laser ablation (U-Th-Sm)/He dating of detrital apatite. *Chem. Geol.* **548**, 119683 (2020).
90. S. C. Boone, C. Seiler, B. P. Kohn, A. J. W. Gleadow, D. A. Foster, L. Chung, Influence of Rift Superposition on Lithospheric Response to East African Rift System Extension: Lapur Range, Turkana, Kenya. *Tectonics* (2018), doi:10.1002/2017TC004575.
91. S. C. Boone, B. P. Kohn, A. J. W. Gleadow, C. K. Morley, C. Seiler, D. A. Foster, L. Chung, Tectono-thermal evolution of a long-lived segment of the East African Rift System: Thermochronological insights from the North Lokichar Basin, Turkana, Kenya. *Tectonophysics*. **744**, 23–46 (2018).
92. S. C. Boone, B. P. Kohn, A. J. W. Gleadow, C. K. Morley, C. Seiler, D. A. Foster, Birth of the East African Rift System: Nucleation of magmatism and strain in the Turkana Depression. *Geology*. **47** (2019), doi:10.1130/G46468.1.
93. D. A. Foster, A. J. W. Gleadow, The morphotectonic evolution of rift-margin mountains in central Kenya: Constraints from apatite fission-track thermochronology. *Earth Planet. Sci. Lett.* **113**, 157–171 (1992).
94. A. J. W. Gleadow, Fission track age of the KBS Tuff and associated hominid remains in northern Kenya. *Nature*. **284**, 225–230 (1980).
95. W. P. Noble, thesis, La Trobe University (1997).
96. D. A. Majer-Kielbaska, thesis, University of Melbourne (2015).
97. M. Wagner, R. Altherr, P. Van Den Haute, Apatite fission-track analysis of Kenyan basement rocks: constraints on the thermotectonic evolution of the Kenya dome. A

reconnaissance study. *Tectonophysics*. **204**, 93–110 (1992).
98. E. Abbate, M. L. Balestrieri, G. Bigazzi, Morphostructural development of the Eritrean rift flank (southern Red Sea) inferred from apatite fission track analysis. *J. Geophys. Res.* **107**, 1–12 (2002).
99. B. P. Kohn, S. Feinstein, D. A. Foster, M. S. Steckler, M. Eyal, Thermal history of the eastern Gulf of Suez, II. Reconstruction from apatite fission track and 40Ar/39Ar K-feldspar measurements. *Tectonophysics*. **283**, 219–239 (1997).
100. B. Kohn, T. Weissbrod, L. Chung, K. Farley, S. Bodorkos, Low-temperature thermochronology of francolite: Insights into timing of Dead Sea Transform motion. *Terra Nov.* **31**, 205–219 (2019).
101. M. A. Menzies, J. Baker, D. Bosence, C. Dart, I. Davison, A. Hurford, M. Al'Kadasi, K. McClay, G. Nichols, A. Al'Subbary, A. Yelland, The timing of magmatism, uplift and crustal extension: Preliminary observations from Yemen. *Geol. Soc. Spec. Publ.* **68**, 293–304 (1992).
102. M. Menzies, K. Gallagher, A. Yelland, A. J. Hurford, Volcanic and nonvolcanic rifted margins of the Red Sea and Gulf of Aden: Crustal cooling and margin evolution in Yemen. *Geochim. Cosmochim. Acta*. **61**, 2511–2527 (1997).
103. N. Morag, I. Haviv, M. Eyal, B. P. Kohn, S. Feinstein, Early flank uplift along the Suez Rift: Implications for the role of mantle plumes and the onset of the Dead Sea Transform. *Earth Planet. Sci. Lett.* **516**, 56–65 (2019).
104. D. Naylor, M. Al-Rawi, G. Clayton, M. J. Fitzpatrick, P. F. Green, Hydrocarbon potential in Jordan. *J. Pet. Geol.* **36**, 205–236 (2013).
105. G. I. Omar, B. P. Kohn, T. M. Lutz, H. Faul, The cooling history of Silurian to Cretaceous alkaline ring complexes, south Eastern Desert, Egypt, as revealed by fission-track analysis. *Earth Planet. Sci. Lett.* **83**, 94–108 (1987).
106. G. I. Omar, M. S. Steckler, W. R. Buck, B. P. Kohn, Fission-track analysis of basement apatites at the western margin of the Gulf of Suez rift, Egypt: evidence for synchroneity of uplift and subsidence. *Earth Planet. Sci. Lett.* **94**, 316–328 (1989).
107. E. Szymanski, D. F. Stockli, P. R. Johnson, C. Hager, Thermochronometric evidence for diffuse extension and two-phase rifting within the Central Arabian Margin of the Red Sea Rift. *Tectonics*. **35**, 2863–2895 (2016).
108. P. Vermeesch, D. Avigad, M. O. McWilliams, 500 Myr of thermal history elucidated by multi-method detrital thermochronology of North Gondwana Cambrian sandstone (Eilat area, Israel). *Bull. Geol. Soc. Am.* **121**, 1204–1216 (2009).
109. E. Abbate, M. L. Balestrieri, G. Bigazzi, Uplifted rift-shoulder of the Gulf of Aden in northwestern Somalia: Palinspastic reconstructions supported by apatite fission-track data. *Mémoires du Muséum Natl. d'histoire Nat.* **186**, 629–640 (2001).
110. M. L. Balestrieri, F. M. Stuart, C. Persano, E. Abbate, G. Bigazzi, Geomorphic development of the escarpment of the Eritrean margin, southern Red Sea from combined apatite fission-track and (U–Th)/He thermochronometry. *Earth Planet. Sci. Lett.* **231**, 97–110 (2005).
111. T. Abebe, M. L. Balestrieri, G. Bigazzi, The Central Main Ethiopian Rift is younger than 8 Ma: confirmation through apatite fission-track thermochronology. *Terra Nov.* **22**, 470–476 (2010).
112. M. L. Balestrieri, E. Abbate, G. Bigazzi, O. E. B. Ali, Thermochronological data from Sudan in the frame of the denudational history of the Nubian Red Sea margin. *Earth Surf. Process. Landforms*. **34**, 1279–1290 (2009).
113. A. V. Bojar, H. Fritz, S. Kargl, W. Unzog, Phanerozoic tectonothermal history of the Arabian-Nubian shield in the Eastern Desert of Egypt: Evidence from fission track and paleostress data. *J. African Earth Sci.* **34**, 191–202 (2002).

114. S. Feinstein, M. Eyal, B. P. Kohn, M. S. Steckler, K. M. Ibrahim, B. K. Moh'd, Y. Tian, Uplift and denudation history of the eastern Dead Sea rift fl ank , SW Jordan : Evidence from apatite fi ssion track thermochronometry. *Tectonics*. **32**, 1513–1528 (2013).
115. W. Ghebreab, A. Carter, A. J. Hurford, L. Jouniaux, Constraints for timing of extensional tectonics in the western margin of the Red Sea in Eritrea. *Earth Planet. Sci. Lett.* **200**, 107–119 (2002).
116. B. P. Kohn, M. Eyal, History of uplift of the crystalline basement of Sinai and its relation to opening of the Red Sea as revealed by fission track dating of apatites. *Earth Planet. Sci. Lett.* **52**, 129–141 (1981).